Insight into dynamic magnetic properties of YMnO3/FM bilayer in a time-dependent magnetic field

Chun-lu Chang
Shenyang University of Technology
Wei Wang (ww9803@126.com)
Shenyang University of Technology https://orcid.org/0000-0002-2727-9684
Dan Lv
Shenyang University of Technology
Zhen-yu Liu
Shenyang University of Technology
Ming Tian
Shenyang University of Technology

Research Article

Keywords: YMnO3/FM bilayer, Mixed-spin Ising model, Dynamic order parameter, Phase diagram, Hysteresis loop, Monte Carlo simulation

Posted Date: February 19th, 2021

DOI: https://doi.org/10.21203/rs.3.rs-229850/v1

Version of Record: A version of this preprint was published at The European Physical Journal Plus on March 4th, 2021. See the published version at https://doi.org/10.1140/epjp/s13360-021-01280-8.

Insight into dynamic magnetic properties of $YMnO_3$/FM bilayer in a time-dependent magnetic field

Chun-lu Chang, Wei Wang*, Dan Lv, Zhen-yu Liu, Ming Tian

School of Sciences, Shenyang University of Technology, Shenyang, China, 110870

*Corresponding author: Wei Wang, *E-mail address*: ww9803@126.com

Abstract

Based on the Monte Carlo simulation, a mixed-spin (5/2, 2, 3/2) Ising model is constructed to investigate the dynamic magnetic properties of antiferromagnetic/ferromagnetic $YMnO_3$/FM bilayer under the existence of a time-dependent magnetic field. The effects of exchange interaction, oscillating magnetic field as well as temperature are involved in this work. Masses of numerical results of the dynamic order parameter, susceptibility, internal energy, and blocking temperature are obtained with diverse physical parameters. Moreover, the phase diagrams and the hysteresis loops of the system are discussed in detail as well for a better understanding of the dynamic properties of the present system.

Keywords: $YMnO_3$/FM bilayer; Mixed-spin Ising model; Dynamic order parameter; Phase diagram; Hysteresis loop; Monte Carlo simulation

1. Introduction

Multifunctional ceramics material, a kind of functional materials with rich application, has received extensive attention and numerous research results in the past decades [1-2]. In particular, multiferroics, a member of the multifunctional material family, have been the protagonist of the studies because of the coexistence of electric and magnetic orders in this material and some specific natural properties, which guarantees the comprehensive applications in multifunctional nanodevices, e.g. multiple-state memory devices, magnetoelectric transformers, and tunable microwave devices [3-5]. With the development of technology, a novel type of multiferroic material has been discovered that is $YMnO_3$. $YMnO_3$ is a one-multiferroic compound with perovskite crystal structure and it can exhibit antiferromagnetism and ferroelectricity in magnetic field and electric field, respectively, at room temperature[6-8]. The response of multiferroic thin films to magnetic and electric fields is similar with that. Experimentally, antiferromagnetic/ferromagnetic (AFM/FM) materials such as $YMnO_3$-based composites have been successfully prepared applying multiple methods, for instance, sol-gel method [9], solid-state reaction method [10], and dp-coating [11].

On the other hand, it goes without saying that masses of experimental phenomena should be analyzed from a theoretical point of view, which can better explain the experimental results and provide a feasible direction for further experiments. As an important role in the field of multiferroic materials, the AFM/FM

composites are also widely studied in theory. By means of Monte Carlo simulation based on Metropolis algorithm, a theoretical calculation was implemented to study the ground-state phase diagrams and the hysteresis circles of the perovskite $YMnO_3$ under the influence of different physical parameters, such as external field, exchange interaction, and crystal field [12]. And a theoretical investigation was performed by Cao to investigate the magnetic entropy change properties of $BiFeO_3$ by dint of quantum microscopic calculations, which depends on the Green's function, Maxwell's relation, and the classical thermodynamical theory [13]. Other theoretical studies were also taken to investigate the properties of such $YMnO_3$ and $BiFeO_3$ multiferroics as well [14, 15].

Recently, much interest has been concentrated on AFM/FM bilayers such as $YMnO_3$/FM and $BiFeO_3$/FM bilayer systems due to their superior application in information storage, gas sensors, spintronic, and solar energy conversion [16-18]. As for such system, lots of theoretical researches were implemented by a large number of scholars majoring in the multiferroics domain. The important properties of a $BiFeO_3$/$YMnO_3$ bilayer was investigated by Masrour using Monte Carlo (MC) simulations [19]. The various electric polarization and hysteresis cycle as the change of the different exchange interaction and magnetic field, as well as the Curie and Neel temperature of the system, were given. Applying the Monte Carlo method and Metropolis dynamics, a simulation of a FM/FE multiferroic bilayer system was performed by Ortiz-Álvarez et al. and aimed to investigate the magnetoelectric interactions of the system [20]. In Refs. [21, 22], Ainane et al. deduced the hysteresis

behaviors and susceptibility under the influence of the exchange interaction and the transverse field of a bilayer system constructing by transverse Ising model. Beyond all doubt, the mixed-spin Ising model is an important theoretical model on the research of low-dimensional ferromagnetism and ferroelectricity materials. To name a few, by establishing the mixed spin (1/2, 1) core/shell structure, the dielectric properties of a nanowire, were examined in Ref. [23]. The dielectric properties of mixed spins ($S = 5/2$ and $\sigma = 2$) model, which is constructed for a nanotube structure were studied by Masrour et al. [24] via MC simulation for several sizes.

When the ferromagnetic and ferroelectric materials were applied to a time-dependent magnetic or electric field, it is practical and interesting to investigate the dynamic properties of these systems theoretically. Deviren et al. investigated the dynamic properties, thermal and hysteresis behaviors, as well as correlations of a cylindrical Ising nanotube under the influence of a time-dependent oscillating magnetic field by EFT and the Glauber-type stochastic dynamics approach [25]. In Ref. [26], a tow-dimensional ferromagnetic kinetic Ising model was established to study the influence of next-nearest neighbor interactions on the system in the presence of external field. It was concluded that this model can perform an interaction induced transition from a deterministic to a stochastic state. For a two-dimensional ferrimagnetic system, the dynamic phase transition temperature, dynamic compensation points as well as dynamic hysteresis behaviors in a oscillating magnetic field were investigated based on dynamic mean-field theory [27]. The nonequilibrium dynamic properties of a mixed-spin ferrimagnetic system with a time-dependent

magnetic field were studied. The phase transition and dynamic critical temperature of the system were discussed in detail [28]. Moreover, unique dynamic magnetic properties were discovered in other mixed-spin systems in the time-dependent magnetic field [29-32].

In our previous works, much effort was made on the magnetic and dielectric properties of the low-dimensional mixed-spin nano-systems using Monte Carlo simulations [33-38]. In addition, such $BiFeO_3$/FM bilayer system was also investigated [39-41]. However, to the best of our knowledge, little energy is devoted to the dynamic properties, such as dynamic order parameter, internal energy, susceptibility, and dynamic hysteresis behaviors of $YMnO_3$/FM systems. Especially, few studies reported the properties of this system in an oscillating magnetic field. Therefore, in this work we investigate the dynamic properties of a mixed-spin (5/2, 2, 3/2) $YMnO_3$/FM bilayer system under the existence of a time-dependent oscillating magnetic field. The organization of the rest part of the article is as follows: In section 2, the model and method are defined. In section 3, the detailed results and discussions are presented. Eventually, a conclusion is included in section 4.

2. Model and Method

We should mention that there are lots of works about the magnetic, dielectric, dynamic properties and hysteresis behaviors of the magnetic or electric low-dimensional nano-systems, which are constructed on various extended mixed-spin Ising systems [42-44]. Therefore, in the present work, we propose a mixed-spin (5/2, 2, 3/2) Ising model to study the dynamic properties of such a

$YMnO_3$/FM bilayer system, which is constructed on the honeycomb lattices in Fig. 1. It consists of the AFM ($YMnO_3$) top layer and the FM bottom layer. The red balls represent the Mn atoms with spin-2 on the top layer, and the green and yellow balls denote the atoms with spin-3/2 (such as Co) and spin-5/2 (such as Fe^{III}) in the bottom layer, respectively. The number of sublattices in each layer and the thickness of the bilayer are described by N and L, respectively. Obviously, the value of L takes L=2 for such a bilayer system. Additional numerical simulations were performed just to determine the definite value of N, no significant difference was found in the simulation results when N changed from 20 to 100. Therefore, in order to save time and reduce the possible errors in a complex simulation process, we decide to set 2×20×20×2 as the number of total sublattices in such bilayer. The Hamiltonian of the system is given as following:

$$H = -J_{ab}\sum_{<i,j>} S_{ia}^{z} S_{jb}^{z} - J_{cd}\sum_{<m,n>} \sigma_{mc}^{z}\mu_{nd}^{z} - J_{ac}\sum_{<i,m>} S_{ia}^{z}\sigma_{mc}^{z} - J_{bd}\sum_{<j,m>} S_{jb}^{z}\mu_{nd}^{z} - h(t)\left(\sum_{i} S_{ia}^{z} + \sum_{j} S_{jb}^{z} + \sum_{m} \sigma_{mc}^{z} + \sum_{n} \mu_{nd}^{z}\right) \quad (1)$$

where, S_{ia}^{z}, S_{jb}^{z}, σ_{mc}^{z} and μ_{nd}^{z} denote the z-components of the Ising spins of sublattices a, b, c and d, respectively. They can take the spin values of $S_{ia(jb)}^{z} = \pm 2, \pm 1, 0$, $\sigma_{mc}^{z} = \pm\frac{3}{2}, \frac{1}{2}$, $\mu_{nd}^{z} = \pm\frac{5}{2}, \pm\frac{3}{2}, \pm\frac{1}{2}$, namely. Here, <...> indicates the summation of nearest-neighbor spins in the same sublattice and between the sublattices located in different adjacent layers. Then, J_{ab}(<0) denotes the intralayer AFM exchange interaction constant between sublattices a and b in the top layer. J_{cd}(>0) represents the FM exchange interaction constant between sublattices c and d in the bottom layer. J_{ac} and J_{bd} are the interlayer exchange interaction constants

between the adjacent sublattices a and b, c, and d, respectively. In this work, the AFM exchange interaction constant J_{ab} was used as the reduced unit of energy and temperature and set $|J_{ab}| = 1$. Finally, the time-dependent oscillating magnetic field is described as:

$$h(t) = h_b + h_0 \sin(\omega t) \tag{2}$$

Where h_b is the bias field of the oscillating field, h_0 and ω stand for the amplitude and the angular frequency of the oscillating magnetic field, respectively.

The numerical method we used in this work for the whole process is the standard importance-sampling MC simulation based on the Metropolis algorithm [45]. In the transverse direction (*x*-*y* plane) of the structure, a periodic boundary condition is taken into account. And in the longitudinal direction (*z*-axis), a free boundary condition is applied. The following is a description of the quantities we care about in this work.

The instantaneous sublattice magnetizations per spin, which are named as M_a, M_b, M_c, and M_d are described as：

$$M_a(t) = \frac{1}{2 \times N \times N} < \sum_i S_{ia}^z > \tag{3}$$

$$M_b(t) = \frac{1}{2 \times N \times N} < \sum_j S_{jb}^z > \tag{4}$$

$$M_c(t) = \frac{1}{2 \times N \times N} < \sum_m \sigma_{mc}^z > \tag{5}$$

$$M_d(t) = \frac{1}{2 \times N \times N} < \sum_n \mu_{nd}^z > \tag{6}$$

and the instantaneous magnetization of the total system per spin M is:

$$M(t) = \frac{M_a(t) + M_b(t) + M_c(t) + M_d(t)}{4} \tag{7}$$

Thus, the average dynamic order parameter per spin can be calculated by:

$$Q = \frac{\omega}{2\pi} \oint M(t) dt \tag{8}$$

The dynamical average internal energy per spin U is shown as:

$$U = \frac{\omega}{2\pi} \oint H(t) dt \tag{9}$$

Finally, the susceptibility χ of the system per spin is:

$$\chi = N^2 \frac{L}{2} \beta (< Q^2 > - < Q >^2) \tag{10}$$

here $\beta = \frac{1}{k_B T}$, where k_B and T represents the Boltzmann constant and the absolute temperature, respectively. In this work, we select $k_B = 1$ for the convenience of calculation.

3. Simulation results and discussions

3.1 Dynamic order parameter, susceptibility, internal energy, and phase diagrams

In this subsection, the dynamic order parameter(Q), susceptibility(χ), internal energy(U), and the blocking temperature(T_B) of the present AFM/FM mixed-spin system under the influence of the intralayer and interlayer exchange interactions as well as the intrinsic parameters(h_b, h_0, ω) of the time-dependent oscillating magnetic field $h(t)$ were presented.

Firstly, for the fixed values of J_{cd} = 0.1, J_{bd} = -0.5, ω = 0.02π, h_0 = 1.0 and h_b = 0.5, the influence of J_{ac} on the Q, χ, U, and the blocking temperature T_B are presented. In Fig. 2(a), six smooth curves are plotted in the (Q, T) plane for different values of J_{ac} changed from 0.1 to 2.1. There is a noteworthy phenomenon that is just one saturation (Q = 1.0) is observed when T is near zero and every Q curve has the similar trend, that is, for lower T, all of them decrease slowly, and then decrease sharply with

the increase of T, finally, stabilizing at a constant value because of the existence of bias magnetic field h_b. Moreover, at a certain T, the lager J_{ac} is beneficial to the increase of Q. The similar behaviors of Q curves can be seen in the mixed spin-1/2 and spin-3/2 ferrimagnetic system [28] and a nano-graphene [31]. All of these results mentioned above indicate that changes in intralayer exchange interaction J_{ac} do not easily cause changes in the spin state of the system. Fig. 2(b) illustrates the U curves of the system. As it can be seen, all curves have a smooth trend from small to large. And at a certain T, as J_{ac} goes up, U goes down. This phenomenon can be physically explained that when J_{ac} increases, the mutual binding force between the spins of the system would be greater, and obviously, the energy in the system would be reduced. Similar phenomenon of U curves can be seen in Refs. [36, 37, 41]. The χ curves of the system is displayed in Fig. 2(c), as shown in the figure, every curve has a peak which corresponds to a certain temperature, which is called the blocking temperature T_B [41]. Obviously, the peak of the curve moves to right with increasing J_{ac}. The explanation of this phenomenon is similar to that of the internal energy curve from a theoretical point of view, that is, an increase in the mutual constraint between the spins due to an increase in J_{ac} will also increase the T_B because the spins need a greater energy to flip. Finally the phase diagram is shown in Fig. 2(d). It can be seen that the relation between T_B and J_{ac} is almost linear, which is similar to the relation between T_B and exchange interaction in Refs. [29, 37].

Fig. 3(a)-(d) presents the Q, U, χ, and phase diagram under the influence of J_{bd} on the condition of $J_{cd} = 1.0$, $J_{ac} = 0.8$, $\omega = 0.02\pi$, $h_0 = 1.0$ and $h_b = 0.5$. When $3 \leq T \leq$

10, six Q curves are clearly seen and the values of them become greater as J_{cd} increases at a certain temperature, which is also seen in Fig. 2(a). Six U curves, which are similar to that in Fig. 2(b) is plotted in Fig. 3(b), the big difference between them is J_{bd} has a more obvious influence on U than J_{ac}, which can be summarized from the relatively dispersed curves in Fig. 3(b). The χ curves are presented in Fig. 3(c) and the change in T_B under the influence of J_{bd} is shown in fig. 3(d). We should mention that there exists a sharp decrease in the T_B curve when $J_{bd} \leq$ -1.5. Actually, with the gradual decrease of the absolute value of J_{bd}, most of the spins bounded by the exchange interaction are released and reverse in a higher energy state, so T_B will decrease sharply correspondingly. These have a high degree of similarity to the results in Refs. [19-21, 43, 46].

Then, let us discuss the effect of interlayer exchange interaction J_{cd} on the Q, U, χ, T_B of the system with the fixed values of J_{ac} = 0.8, J_{bd} = -0.5, $\omega = 0.02\pi$, h_0 = 1.0 and h_b = 0.5. As shown in Fig. 4(a), the shape of all Q curves are the same as that shown in Fig. 2(a) and Fig. 3(a). A phenomenon should be noticed that when T is lower ($T \leq 1$), all Q curves tend to be constant, and as J_{cd} increases, the temperature range corresponding to a constant Q continuously increases, such as when J_{cd} is 2.0, the temperature range is about $0 \leq T \leq 5$. From a physical point of view, Q exists under the competition between temperature, exchange interaction and magnetic field, and the larger J_{cd} is more dominant in the competition among the three. It can bind the spin to a fixed state which is not easy to change, thus leading to the stability and invariability of Q [33-38, 41]. In Fig. 4(c), an interesting phenomenon has been

observed that there is a maximum in the low-temperature zone in the χ curve labeled J_{cd}=0.1, which is the result of the rapid drop in the Q in Fig.4(a). The T_B curve is shown in Fig. 4(d) and as J_{cd} increases, T_B goes up continuously and slowly, and then goes straight up when J_{cd} reaches 1.0, which obviously means that larger J_{cd} is more conducive to the stability of the system.

The following three Figs. 5-7 describe various magnetic properties of the system under the effects of the intrinsic parameters of the time-dependent oscillating magnetic field. First of all, Fig. 5(a)-(d) reveals the variation of Q, U, χ, and T_B under the influence of h_b with J_{cd} = 1.0, J_{ac} = 0.8, J_{bd} = -0.5, ω = 0.02π and h_0 = 1.0. Obviously, in Fig. 5(a), these Q curves have different values when the temperature is high, which originates from the existence of a bias magnetic field h_b. Some similar results with this phenomenon are shown in Refs. [31, 47, 48]. When the temperature is low and h_b is greater than 1.8, a maximum appears on the Q curve and increases with the increase of h_b. This fact can be attributed to fluctuations in temperature [49, 50]. As shown in Fig. 5(b), the augment of h_b is advantageous for the enlargement in U. Fig. 5(c) and (d) reflect the influence of the change of h_b on T_B. For visual intuition and convenience of expression, we discuss Fig. 5(d) directly. An amazing phenomenon is discovered in the (h_b, T_B) plane, that is, T_B increases as h_b increases, and the relationship is almost linear, which is the opposite of the behavior of T_B under exchange interactions (see Figs. 2(d), 3(d), 4(d)). The reason for this is that the increase of h_b would enhance the magnetic order of the system, therefore, to break this order, more thermal energy is needed so that it can reach the paramagnetic phase.

Thus, as we expected, T_B increases as h_b increases. A comparison is made with those in Ref. [41], and there is a high similarity between the two in the effect of bias field on T_B.

Next, Fig. 6(a)-(c) shows the Q, U, χ as a function of T for selected h_0 with other parameters J_{cd} = 1.0, J_{ac} = 0.8, J_{bd} = -0.5, ω = 0.02π, h_b = 0.5, and Fig. 6(d) is about the phase diagram displayed in the (h_0, T_B) plane. In Fig. 6(a), it is so clear that all Q curves start with the same constant and also end up with the same constant, which is different from the result obtained in Fig. 5(a) under the influence of h_b. As shown in Fig. 6(b), there exists a fluctuation in the U curves when T is lower. In the perspective of theoretical, when the temperature is low, h_0 is dominant in the competition with the temperature, and it has a greater influence on the thermodynamic properties of the system, thus causing thermal agitation of the system at low temperature. Fig. 6(c) is the χ curves of the system, and Fig. 6(d) is an intuitive phase diagram. Just as we expected, a continuous increase in h_0 will cause a gradual decrease in T_B. As we all know, h_0 is the amplitude of the period oscillating magnetic field, and it has a direct contribution to the disorder of the system. Thus, the greater h_0 is, the less stable the system is. And this means that the system needs a lower temperature in paramagnetic phase. We should mention that some other studies also discuss the results, which is similar to above, in detail [28, 31, 32, 47, 51].

Finally, Fig. 7(a)-(d) exhibits the effect of ω on the Q, U, χ, and T_B investigated with selected values of J_{cd} = 1.0, J_{ac} = 0.8, J_{bd} = -0.5, h_0 = 1.0, h_b = 0.5. As Fig. 7(a) shows, Q is sensitive to ω only over a very small temperature range ($4 \leq T \leq 7$), and

increases with the increase of ω, however, when the temperature is relatively low ($T <$ 4) and relatively high ($T > 7$), the change of ω affects Q very slightly. Apparently, for relatively small ω ($\omega = 0.008\pi$), the oscillating magnetic field has a long period acting on the system and relaxes the system easily to undergo phase transition, so the T_B is lower. On the contrary, a relatively large ω means that a short period applies to the present system, weakening the influence of the oscillating magnetic field on the system and making the system keep order longer, so the T_B becomes higher. The similar phenomenon is also shown in the study about nano-graphene bilayer [28], two-dimensional square lattice [32], and double-layer cor-shell graphene nanoisland [52]. Next, turn our attention to Fig. 7(b), there is an apparent result that ω has a negligible effect on U. In order to have a more detailed observation, we enlarge the figure partially, and find that ω helps to improve U comes into our eyes. From Fig. 7(c), we can infer the influence of ω on T_B, and Fig. 7(d) is a figure about the change of T_B under the influence of ω and the increase of ω will cause T_B to increase continuously.

3.2 Hysteresis loops

Fig. 8 presents hysteresis loops of the system under the influence of various exchange interactions with the fixed parameters of $h_0 = 1.0$, $\omega = 0.02\pi$, $T = 0.05$. Firstly, four loops of the same area are observed in Fig. 8(a), which illustrates that J_{ac} has little effect on the hysteresis loops for fixed values of $J_{bd} = -0.5$ and $J_{cd} = 1.0$. While, the effect of J_{bd} on it, which is shown in Fig. 8(b) with fixed $J_{ac} = 0.8$ and $J_{cd} = 1.0$, is more stranger than J_{ac}. As we can see, when J_{bd} increases from -0.1 to -2.0, the

area of the loops get bigger first and than stay stable for J_{bd} = -1.4, which means a larger J_{bd} will not make a significant change in loop. Then, let focus the effect of J_{cd} on hysteresis loop in Fig. 8(c) with the other two values J_{ac} = 0.8 and J_{bd} = -05. It should be emphasized that different from the two Figs. 8(a) and (b), the area of the loop has been changed and the area of the loop increases continuously and it does not stay at a constant as J_{cd} changes from 0.1 to 2.0, which is not similar to that in Fig. 8(b). In these sub-figures above, only single-loop hysteresis behavior can be found, but there are no double loops or more multiple loops, the only thing that changes is the area of the loops, which is similar to the results about it in Refs. [27, 53, 54]. We can conclude that the effects of the exchange interactions on the hysteresis loop of the system are J_{cd}, J_{bd}, J_{ac} in order from small to large.

Fig. 9(a)-(b) shows the influence of the intrinsic characters ω and h_0 of the time-dependence oscillating field on hysteresis loop for fixed J_{cd} = 1.0, J_{ac} = 0.8, J_{bd} = -0.5, and T = 0.05. In Fig. 9(a), when ω is 0.02π, an interesting behavior is seen that the increase of the amplitude h_0 will decrease the area of the loops, which is different from the results under the influence of exchange interaction exhibited in Fig. 8. And Fig. 9(b) is about the impact of ω on the hysteresis behavior when E_0 is 1.0. The similar behavior that is observed in Fig. 8(a) exhibits in Fig. 9(b) again, that is, no matter how ω changes, the area, number and shape of hysteresis loop will not change significantly.

Lastly, we discuss the temperature dependence of the hysteresis loop for other parameters are J_{cd} = 1.0, J_{ac} = 08, J_{bd} = -0.5, ω = 0.02π, and h_0 = 1.0. In Fig. 10(a)-(f),

the area of the loops decreases with T increasing from 0.05 to 3.9, it can be concluded that T has a negative effect on the dynamic hysteresis loops. Ultimately, the loop vanishes when $T \geq 3.9$, which indicates the system turning into paramagnetic phase. As far as we all know, the increase of T can magnify the disorder of the system and dominates the competition among the exchange interaction and the magnetic field, resulting in the diminution in the area of loops and the appearance of the paramagnetic phase of the system. Similar results are found in some other researches, such as the investigations about the ferroelectric or ferrielectric materials [23, 44], $BiFeO_3/YMnO_3$ bilayer [39, 40], $BiFeO_3$/Co bilayer [41], and some magnetic materials [38, 55-58].

4. Conclusion

In summary, in this paper, we successfully study the dynamic properties including dynamic magnetic properties, phase transition as well as hysteresis loops of an Ising mixed-spin (5/2, 2, 3/2) $YMnO_3$/FM bilayer system under the existence of a time-dependent oscillating magnetic field applying Monte Carlo simulation. The effects of the exchange interaction and the external time-dependent magnetic field on the dynamic properties of the present system are discussed in detail. The results reveal that all the parameters we studied have a significant influence on the Q of the system. Except for ω, other parameters also have significant effects on U, which gradually decreases with the increase of absolute values of the parameters. T_B can be improved by increasing J_{ac}, J_{ab}, h_b, and ω, but the increase in h_0 and the decrease in the absolute value of J_{bd} will make T_B go down. Moreover, the rich hysteresis loops are found,

coming from the competition among the exchange interaction, temperature, and time-dependent oscillating magnetic field. We genuinely hope that our theoretical research results can provide references for other theoretical and experimental research on AFM/FM bilayer.

Acknowledgement

This project was supported by the General Project of Liaoning Provincial Department of Education, China (Grant No. LJGD2019013), and National College Students Innovation and Entrepreneurship Training Program (Grant No. 202010142012).

Data availability statements

The raw data that support the findings of this study cannot be shared because it is related to some of the research we are currently conducting, so we will not disclose these raw data based on privacy considerations.

References:

1. S.H. Baek, H.W. Jang, C.M. Folkman, Y.L. Li, B. Winchester, J.X. Zhang, Q. He, Y.H. Chu, C.T. Nelson, M.S. Rzchowski, X.Q. Pan, R. Ramesh, L.Q. Chen, C.B. Eom, Nature Mater. **9**, 309 (2010).

2. T. Choi , Y. Horibe , H.T. Yi , Y.J. Choi , W. Wu , S.W. Cheong, Nat. Mater. **9**, 253 (2010).

3. R. Ramesh, N.A. Spald in, Nat. Mater. **6**, 21 (2007).

4. G. Catalan, J.F. Scott, Adv. Mater. **21**, 2463 (2009).

5. Y. Zhang, Z. Li, C.Y. Deng, J. Ma, Y.H. Lin, C.W. Nan, Appl. Phys. Lett. **92**, 152510 (2008).

6. S.B. Cheng, M.L. Li, S.Q. Deng, S.Y. Bao, P.Z. Tang, W.H. Duan, J. Ma, C. Nan, J. Zhu, Adv. Funct. Mater. **26**, 3589 (2016).

7. S.C. Abrahams, Acta Cryst. **57**, 485 (2001).

8. R. Safi, H. Shokrollahi, Prog. Solid State Chem. **40**, 6 (2012).

9. O. Nirmala, P.S. Reddy, V.D. Reddy, Mater. today **23**, (2019).

10. Y. Ma, X.T. Wang, Z.F. Wang, Q. Zhou, C.Y. Yang, RARE METAL MAT ENG **44**, 52 (2015).

11. H. Kitahata, K. Tadanaga, T. Minami, N. Fujimura, T. Ito, J. Am. Ceram. Soc. **81**, 1357 (1998).

12. N.E. Mekkaoui, S. Idrissi, S. Mtougui, I.E. Housni, R. Khalladi, H. Labrim, S. Ziti, L. Bahmad, Appl. Phys. A **9**, 582 (2019).

13. X.S. Cao, J. Alloys Compd. **806**, 1008 (2019).

14. S.A. Nikolaev, V.G. Mazurenko, A.N. Rudenko, Solid State Commun. **164**, 16 (2013).

15. C. Autieri, B. Sanyal, New J. Phys. **16**, 113031 (2014).

16. C. Moure, M. Villegas, J.F. Fernandez, J. Tartaj, P. Duran, J. Mater. Sci. **34**, 2565 (1999).

17. S. Roy, S.B. Majumder, J. Alloys Compd. **538**, 153 (2012).

18. J.F. Scott, Nat. Mater. **6**, 256 (2007).

19. A. Jabar, R. Masrour, A. Benyoussef, M. Hamedoun, J. Superconduct. Nov. Magn. **29**, 733 (2016).

20. H.H. Ortiz-Álvarez, C.M. Bedoya-Hincapié, E. Restrepo-Parra Phys. B **454**, 235 (2014).

21. A. Ainane, I. Essaoudi, M. Saber, J. Magn. Magn. Mater. **315**, 132 (2007).

22. Y. Benhouria, I. Essaoudi, A. Ainane, A. Oubelkacem, M. Saber, F. Dujardin, Phys. Scr. **86**, 045704 (2012) .

23. A. Feraoun, A. Zaim, M. Kerouad, J. Phys. Chem. Solid. **96-97**, 75 (2016).

24. T. Sahdane, R. Masrour, A. Jabar, Solid State Commun. **310**, 113851 (2020).

25. B. Deviren, M. Keskin, Phys. Lett. A. **376**, 1011 (2012).

26. W.D. Baez, T. Datta, Physics Procedia. **4**, 15 (2010).

27. M. Ertaş, Superlattices Microstruct. **85**, 734 (2015).

28. E. Vatansever, H. Polat, J. Magn. Magn. Mater. **392**, 42 (2015).

29. M. Keskin, E. Kantar, J. Magn. Magn. Mater. **322**, 2789 (2010).

30. M. Ertaş, M. Keskin, Phys. B. 4**70-471**, 76 (2015).

31. Y. Benhouria, I. Bouziani, I. Essaoudi, A. Ainane, R. Ahuja, J. Magn. Magn. Mater. **460**, 223 (2018).

32. E. Vatansever, U. Akinci, H. Polat, J. Magn. Magn. Mater. **344**, 89 (2013).

33. H.J. Wu, W. Wang, B.C. Li, M. Yang, S.Q. Yang, F. Wang, Phys. E **112**, 86 (2019).

34. M. Yang, W. Wang, B.C. Li, H.J. Wu, S.Q. Yang, J. Yan, Phys. A **539**, 122932 (2020).

35. S.Q. Yang, W. Wang, F. Wang, B.C. Li, H.J. Wu, M.Yang, J.H. Xu, J. Phys. Chem. Solids. **135**, 109110 (2019).

36. H.J. Wu, W. Wang , F. Wang, B.C. Li, Q. Li, J.H. Xu, J. Phys. Chem. Solids. **136**, 109174 (2020).

37. W. Wang, C.L. Chang, Q. Li, F.L. Xue, L. Sun, T. Huang, Superlattices Microstruct. **136**, 106325 (2019).

38. W. Wang, Q. Li, M.Z. Wang, Y. Ma, A.B. Guo, T. Huang, Phys. E **111**, 63 (2019).

39. Z.Y. Wang, Q. Li, F. Wang, L. Sun, M. Tian, W. Wang, Superlattices Microstruct. **136**, 106293 (2019).

40. Z.Y. Wang, W. Wang, Q. Li, M. Tian, Z.Y. Gao, Y. Liu, Phys. E **110**, 127 (2019).

41. C.L. Chang, W. Wang, D. Lv, R.Z. Geng, J.C. Liu, H.Huang, Ceram. Int. **46**, 22907 (2020).

42. A. Jabar, R. Masrour, Sol. Stat. Comm. **268**, 38 (2017).

43. Y. Benhouria, I. Essaoudi, A. Ainane, R. Ahuja, F. Dujardin, Ferroelectrics 5**07**, 58 (2017).

44. A. Feraoun, A. Zaim, M. Kerouad, Sol. Stat. Comm. **248**, 88 (2016).

45. N. Metropolis, A.W. Rosenbluth, M.N. Rosenbluth, A.H. Teller, E. Teller, J. Chem. Phys. **21**, 1087 (1953).

46. E. Kantar, Chin. J. Phys. **55**, 1808 (2017).

47. J.D. Alzate-Cardona, H. Barco-Ríos, E. Restrepo-Parra, Phys. Lett. A **382**, 792 (2018).

48. Y. Benhouria, N. Khossossi, M. Houmad, I. Essaoudi, A. Ainane, R. Ahuja, Phys. E **105**, 139 (2019).

49. H.S.S.R. Matte, K.S. Subrahmanyam, C.N.R. Rao, J. Phys. Chem. C **113**, 9982 (2009).

50. C.N.R. Rao, K.S. Subrahmanyam, H.S.S.R. Matte, B. Abdulhakeem, A. Govindaraj, B. Das, Sci. Technol. Adv. Mater **11**, 054502 (2010).

51. M. Acharyya, J. Magn. Magn. Mater. **323**, 2872 (2011).

52. H.J. Wu, W. Wang, D. Lv, C.L. Chang, B.C. Li, M. Tian, J. Magn. Magn. Mater. **515**, 167306 (2020).

53. L. Wang, B.H. Teng, Y.H. Rong, Y. Lv, Z.C. Wang, Sol. Stat. Comm. **152**, 1641 (2012).

54. E. Vatansever, Phys. Lett. A **381**, 1535 (2017).

55. W. Wang, Q. Li, D. Lv, R.J. Liu, Z. Peng, S. Yang, Carbon **120**, 313 (2017).

56. D. Lv, W. Jiang, Y. Ma, Z. Y. Gao , F. Wang, Phys. E **106**, 101 (2019).

57. D. Lv, Y. Yang, W. Jiang, F. Wang, Z.Y. Gao, M. Tian, Phys. A **514**, 319 (2019).

58. D. Lv, F. wang, R.J. Liu, Q. Xue, S.X. Li, J. Alloys Compd. **701**, 935(2017).

List of figure captions

Fig. 1 Schematic of an antiferromagnetic/ferromagnetic mixed-spin(5/2, 2, 3/2) Ising model with the $YMnO_3$/FM bilayer structure. Four exchange interactions are considered in the structure. J_{ab} and J_{cd} denote the intralayer antiferromagnetic and ferromagnetic exchange interactions of different spins in the top layer between sublattices a and b, and in the bottom layer between sublattices c and d, respectively. J_{ac} and J_{bd} represent the interlayer exchange interactions between sublattices a and c, b and d, namely.

Fig. 2 The temperature dependences of Q, U, χ, and the diagram of T_B for different J_{ac} with $J_{cd} = 1.0$, $J_{bd} = -0.5$, $\omega = 0.02\pi$, $h_0 = 1.0$, and $h_b = 0.5$.

Fig. 3 The temperature dependences of Q, U, χ and the diagram of T_B for different J_{bd} on the condition of $J_{cd} = 1.0$, $J_{ac} = 0.8$, $\omega = 0.02\pi$, $h_0 = 1.0$, and $h_b = 0.5$.

Fig. 4 The temperature dependences of Q, U, χ and the diagram of T_B for different J_{cd} with $J_{ac} = 0.8$, $J_{bd} = -0.5$, $\omega = 0.02\pi$, $h_0 = 1.0$, and $h_b = 0.5$.

Fig. 5 The temperature dependences of Q, U, χ and the diagram of T_B for different h_b with $J_{cd} = 1.0$, $J_{ac} = 0.8$, $J_{bd} = -0.5$, $\omega = 0.02\pi$, and $h_0 = 1.0$.

Fig. 6 The temperature dependences of Q, U, χ and the diagram of T_B for different h_0 with $J_{cd} = 1.0$, $J_{ac} = 0.8$, $J_{bd} = -0.5$, $\omega = 0.02\pi$ and $h_b = 0.5$.

Fig. 7 The temperature dependences of Q, U, χ and the diagram of T_B for different ω with $J_{cd} = 1.0$, $J_{ac} = 0.8$, $J_{bd} = -0.5$, $h_0 = 1.0$ and $h_b = 0.5$.

Fig. 8 The hysteresis loops of the anferromagnetic/ferromagnetic bilayer for different values of (a) J_{ac} with $J_{bd} = -0.5$, $J_{cd} = 1.0$, $h_0 = 1.0$, $\omega = 0.02\pi$, $T = 0.05$, (b) J_{bd} with $J_{ac} = 0.8$, $J_{cd} = 1.0$, $h_0 = 1.0$, $\omega = 0.02\pi$, and $T = 0.05$, (c) J_{cd} with $J_{ac} = 0.8$, $J_{bd} = -0.5$, $h_0 = 1.0$, $\omega = 0.02\pi$, and $T = 0.05$.

Fig. 9 The hysteresis loops of the anferromagnetic/ferromagnetic bilayer for different values of (a) h_0 with $\omega = 0.02\pi$, $J_{cd} = 1.0$, $J_{ac} = 0.8$, $J_{bd} = -0.5$, and $T = 0.05$, (b) ω with $h_0 = 1.0$, $J_{cd} = 1.0$, $J_{ac} = 0.8$, $J_{bd} = -0.5$, and $T = 0.05$.

Fig. 10 The hysteresis loops of the anferromagnetic/ferromagnetic bilayer for different values of T with $J_{cd} = 1.0$, $J_{ac} = 08$, $J_{bd} = -0.5$, $\omega = 0.02\pi$, and $h_0 = 1.0$.

Figures:

Fig. 1

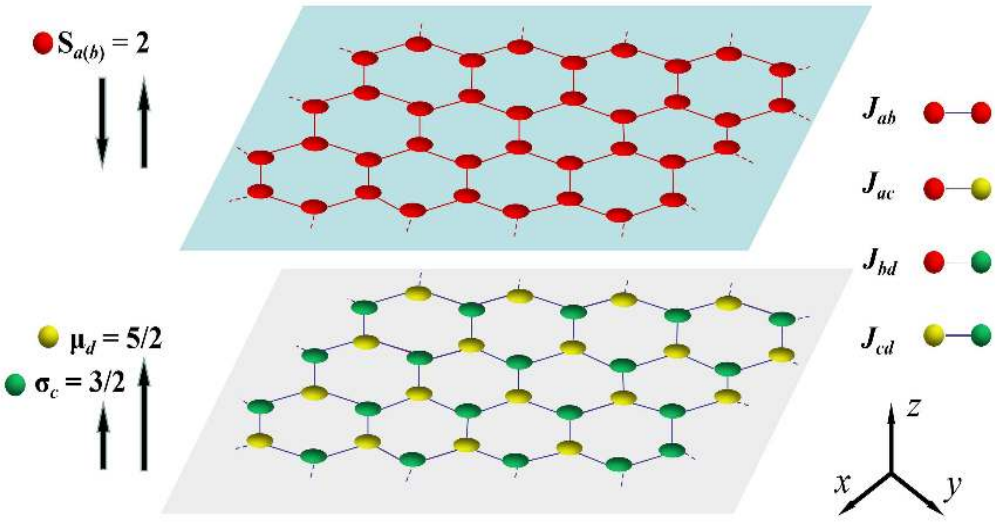

Fig. 2

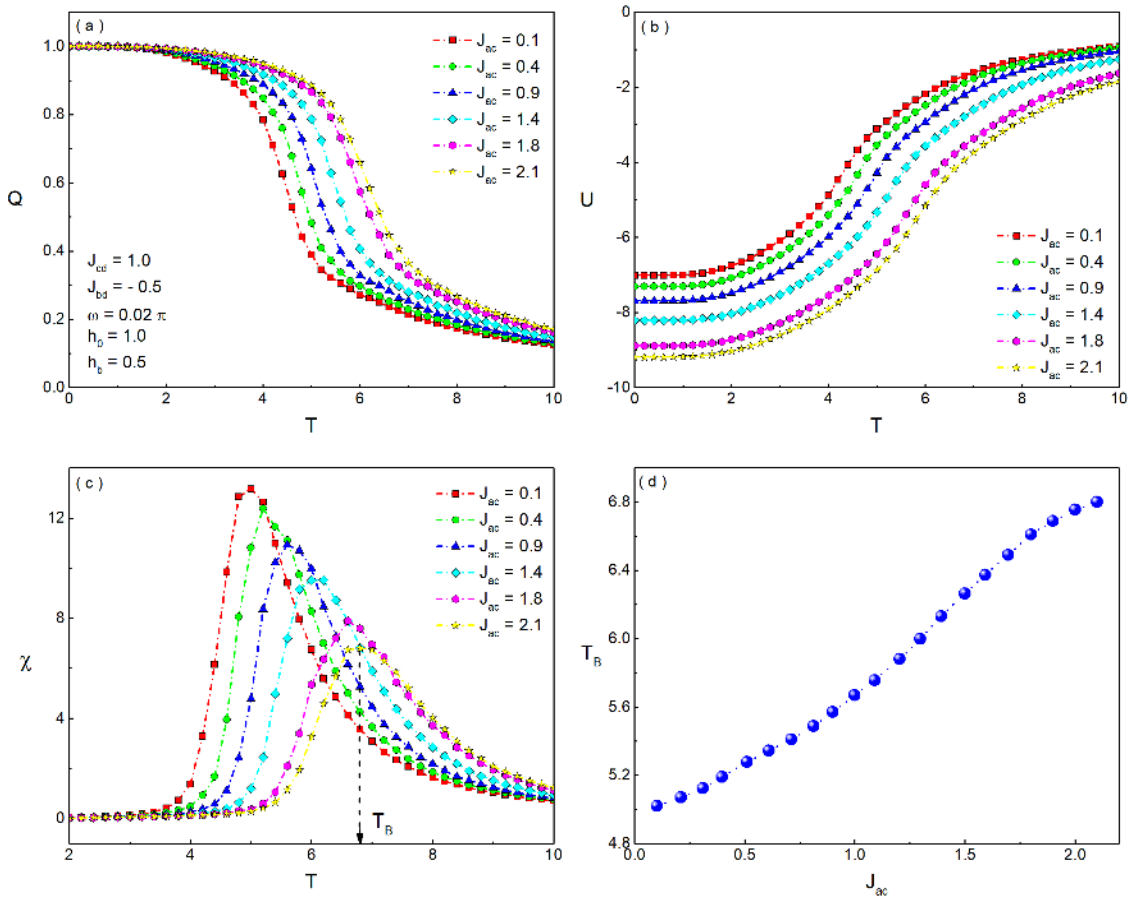
(a)
Q
T
J_{aa} = 1.0
J_{bd} = - 0.5
ω = 0.02 π
h_D = 1.0
h_b = 0.5
J_{ac} = 0.1
J_{ac} = 0.4
J_{ac} = 0.9
J_{ac} = 1.4
J_{ac} = 1.8
J_{ac} = 2.1
(b)
U
T
(c)
χ
T_B
(d)
T_B
J_{ac}

Fig. 3

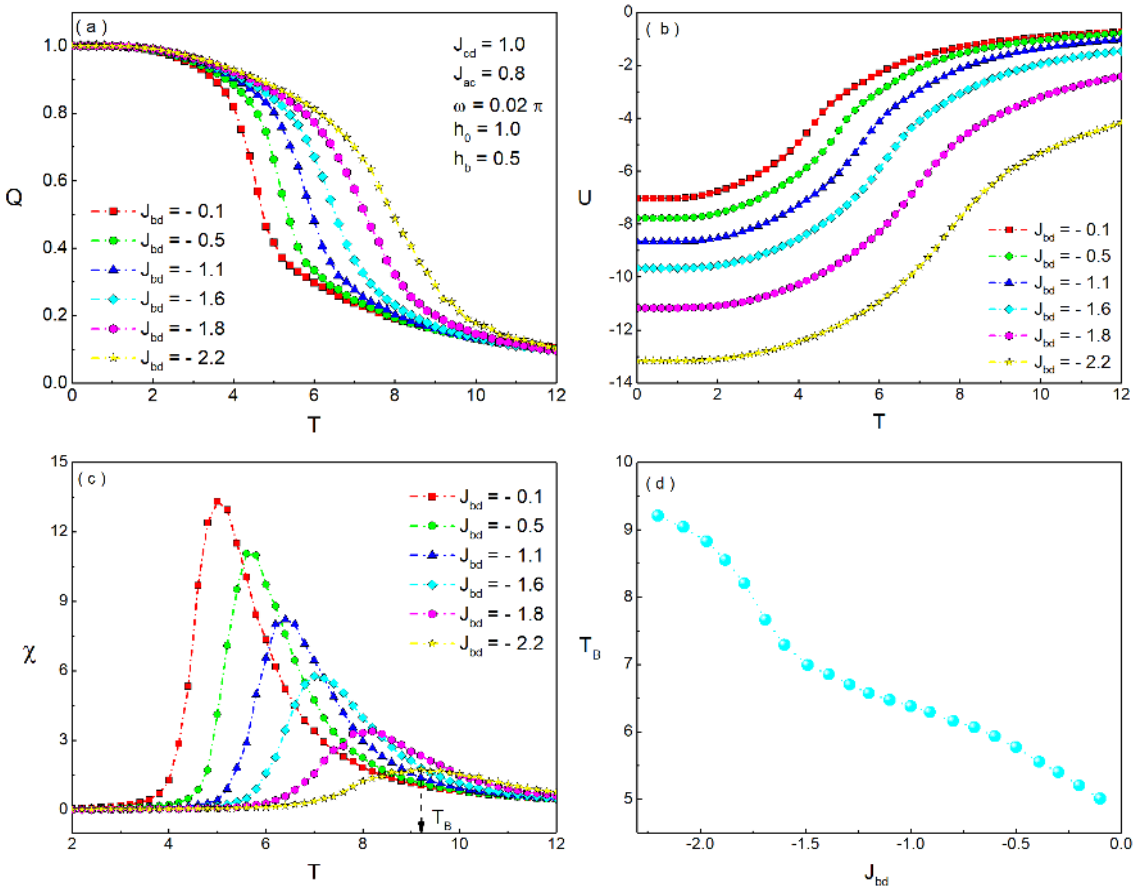
(a)
J_{cd} = 1.0
J_{ac} = 0.8
ω = 0.02 π
h_0 = 1.0
h_b = 0.5
J_{bd} = - 0.1
J_{bd} = - 0.5
J_{bd} = - 1.1
J_{bd} = - 1.6
J_{bd} = - 1.8
J_{bd} = - 2.2
Q
T
(b)
U
T
(c)
χ
T_B
T
(d)
T_B
J_{bd}

Fig. 4

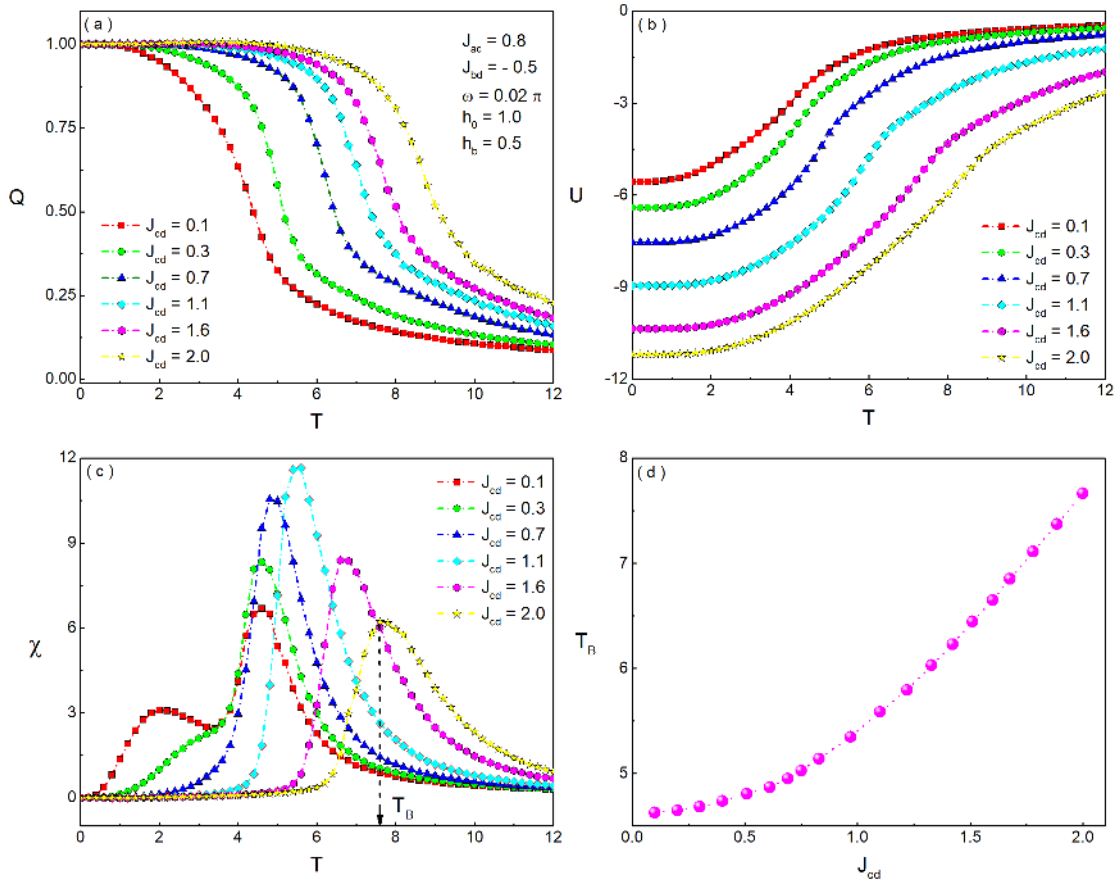
(a)
J_{ac} = 0.8
J_{bd} = - 0.5
ω = 0.02 π
h_0 = 1.0
h_B = 0.5
J_{cd} = 0.1
J_{cd} = 0.3
J_{cd} = 0.7
J_{cd} = 1.1
J_{cd} = 1.6
J_{cd} = 2.0
Q
T
(b)
U
T
(c)
χ
T_B
T
(d)
T_B
J_{cd}

Fig. 5

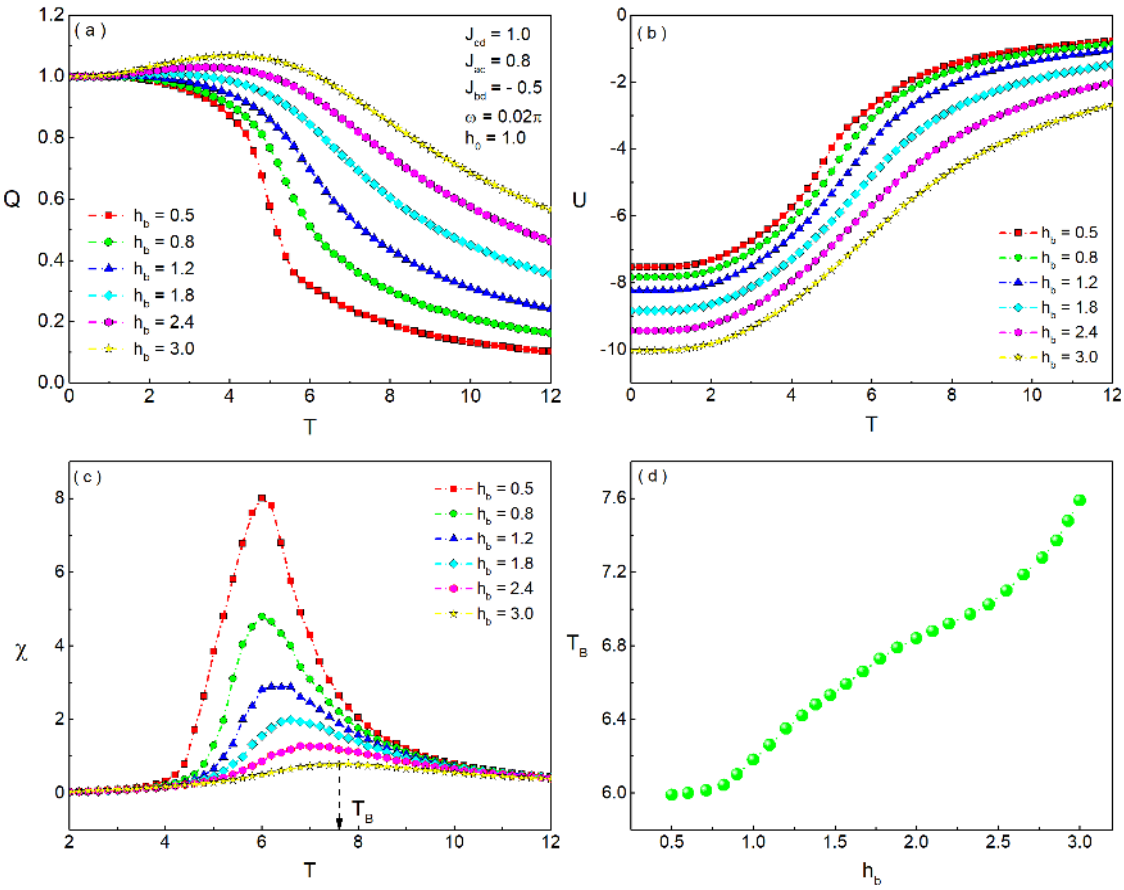
(a)
J_{cd} = 1.0
J_{ac} = 0.8
J_{bd} = - 0.5
ω = 0.02π
h_0 = 1.0
h_b = 0.5
h_b = 0.8
h_b = 1.2
h_b = 1.8
h_b = 2.4
h_b = 3.0
Q
T
(b)
U
T
(c)
χ
T_B
T
(d)
T_B
h_b

Fig. 6

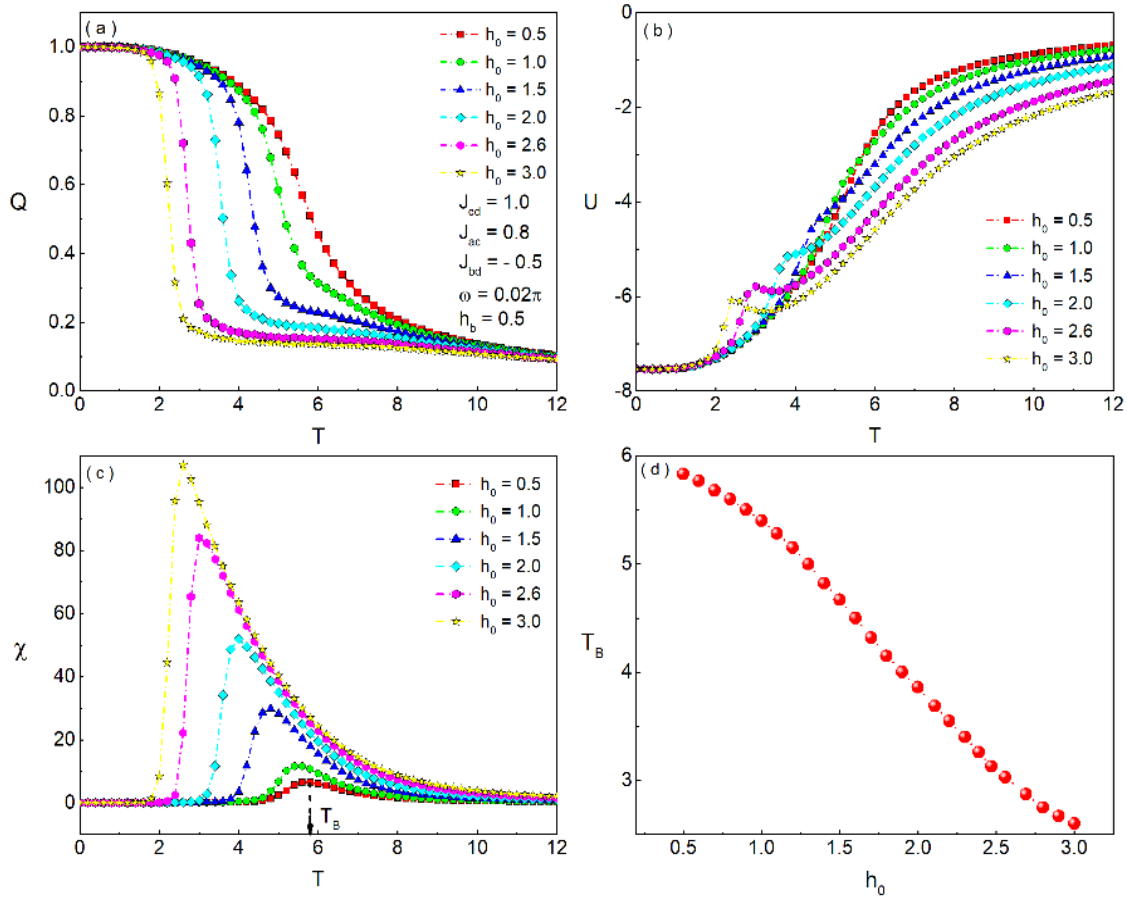
(a)
Q
T
h0 = 0.5
h0 = 1.0
h0 = 1.5
h0 = 2.0
h0 = 2.6
h0 = 3.0
Jcd = 1.0
Jac = 0.8
Jbd = - 0.5
ω = 0.02π
hb = 0.5
(b)
U
T
(c)
χ
T
TB
(d)
TB
h0

Fig. 7

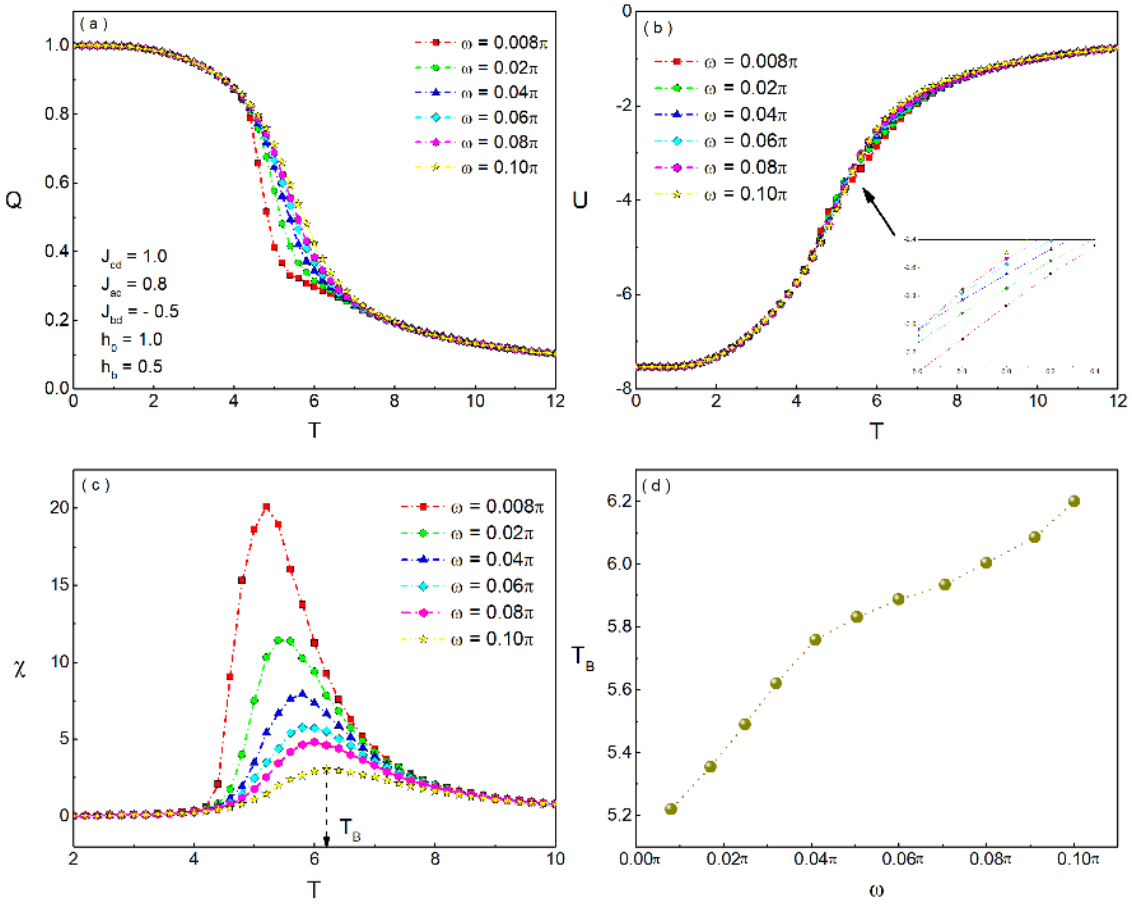
(a)
Q
T
ω = 0.008π
ω = 0.02π
ω = 0.04π
ω = 0.06π
ω = 0.08π
ω = 0.10π
J_cd = 1.0
J_ac = 0.8
J_bd = - 0.5
h_b = 1.0
h_b = 0.5
(b)
U
T
(c)
χ
T
T_B
(d)
T_B
ω
0.00π
0.02π
0.04π
0.06π
0.08π
0.10π

Fig. 8

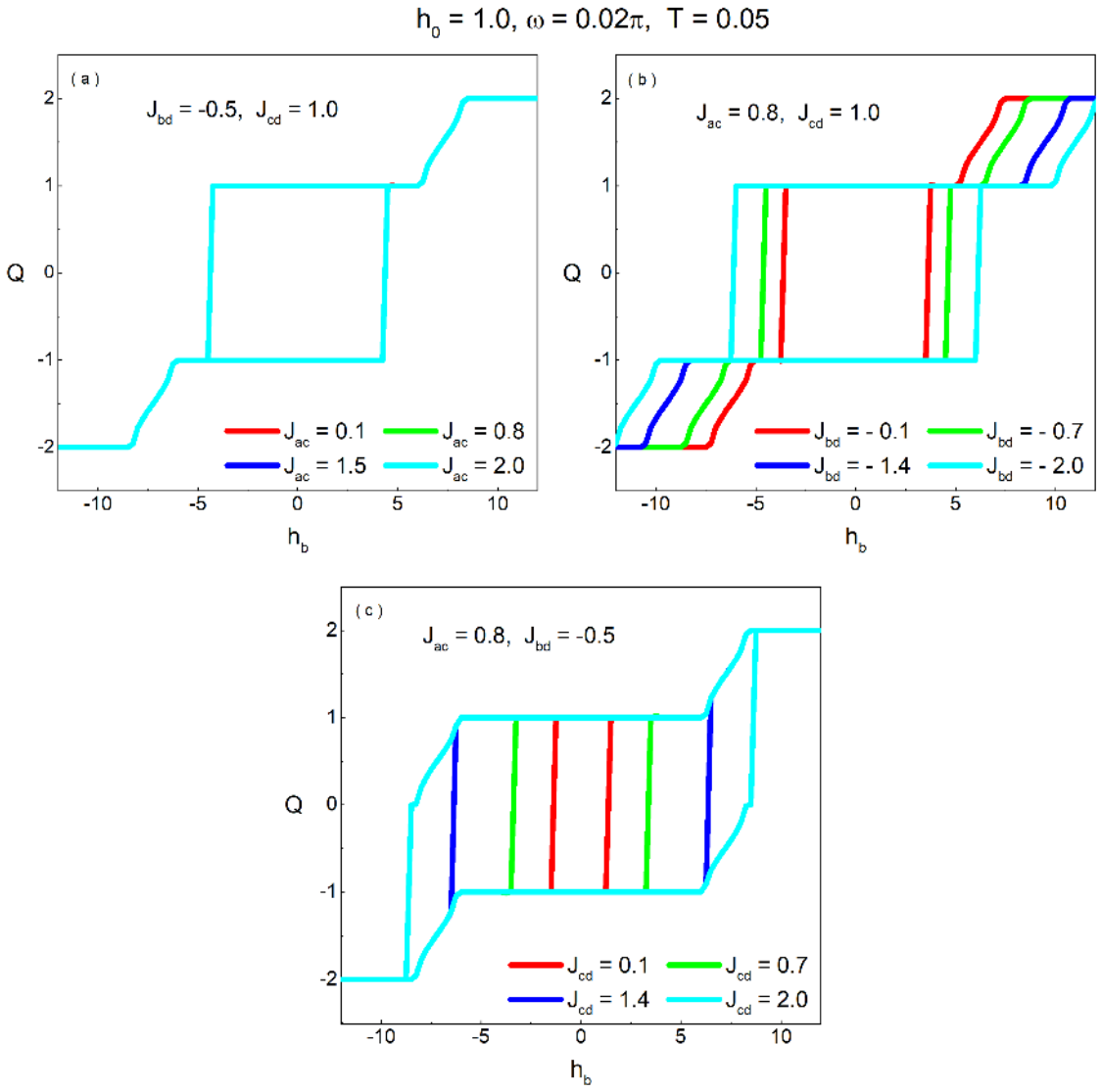
h0 = 1.0, ω = 0.02π, T = 0.05
(a)
Jbd = -0.5, Jcd = 1.0
Jac = 0.1
Jac = 0.8
Jac = 1.5
Jac = 2.0
(b)
Jac = 0.8, Jcd = 1.0
Jbd = - 0.1
Jbd = - 0.7
Jbd = - 1.4
Jbd = - 2.0
(c)
Jac = 0.8, Jbd = -0.5
Jcd = 0.1
Jcd = 0.7
Jcd = 1.4
Jcd = 2.0
Q
hb

Fig. 9

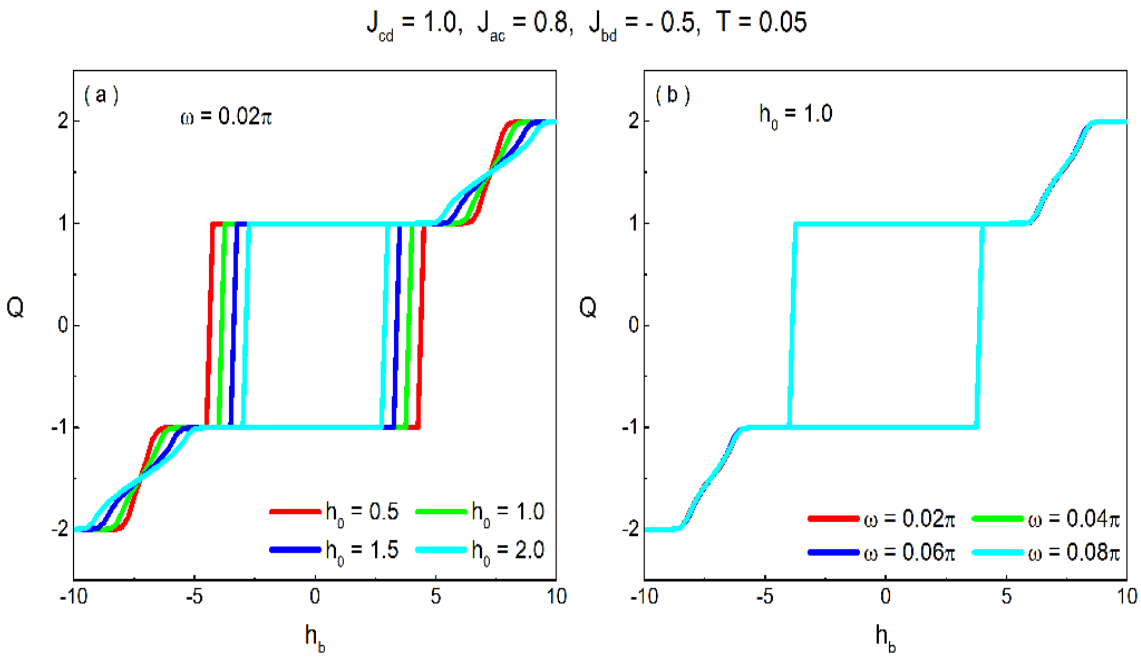
J_cd = 1.0, J_ac = 0.8, J_bd = - 0.5, T = 0.05
(a)
ω = 0.02π
h_0 = 0.5
h_0 = 1.0
h_0 = 1.5
h_0 = 2.0
Q
h_b
(b)
h_0 = 1.0
ω = 0.02π
ω = 0.04π
ω = 0.06π
ω = 0.08π
Q
h_b

Fig. 10

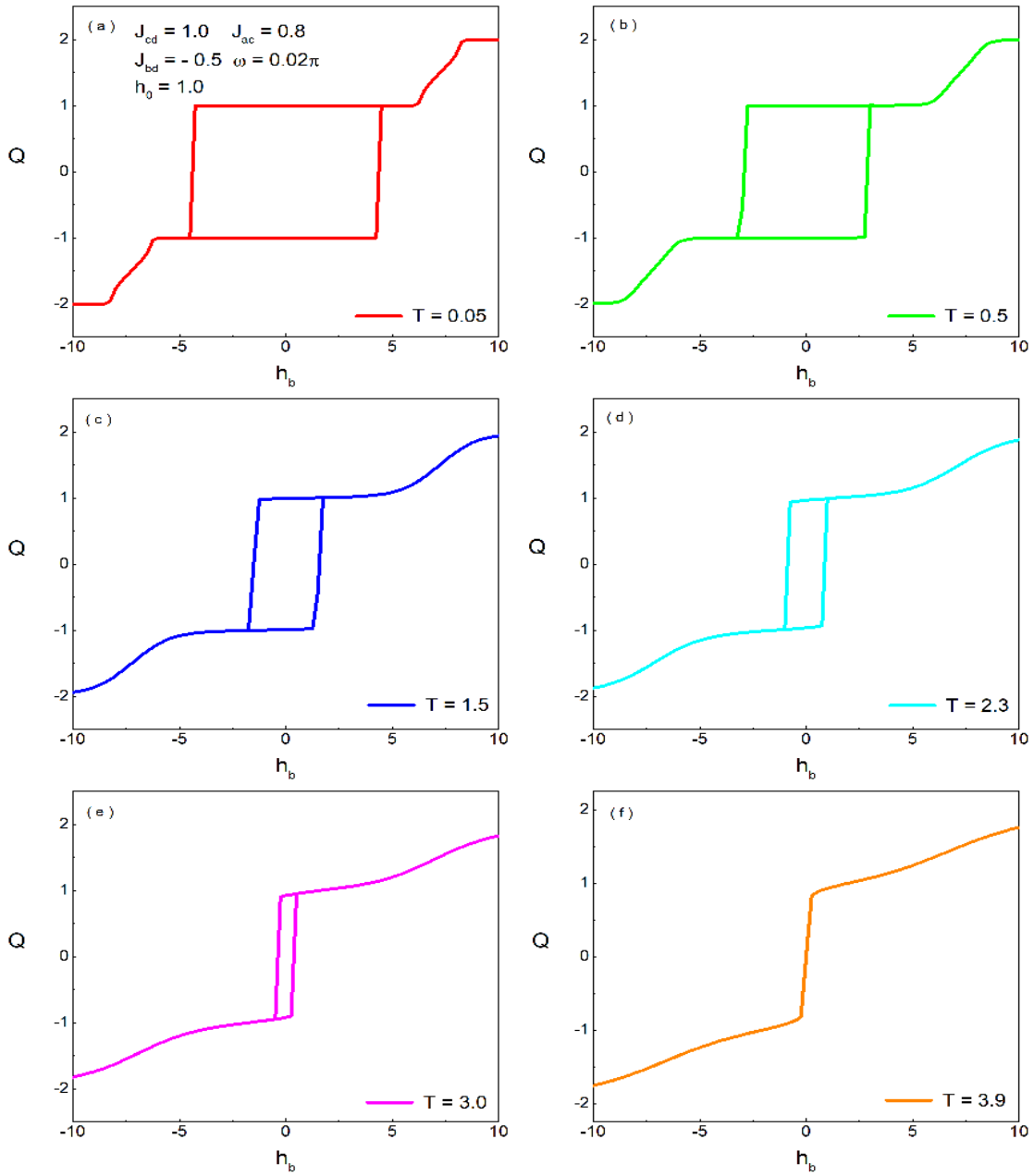
(a) J_{cd} = 1.0 J_{ac} = 0.8
J_{bd} = - 0.5 ω = 0.02π
h_0 = 1.0
T = 0.05
(b)
T = 0.5
(c)
T = 1.5
(d)
T = 2.3
(e)
T = 3.0
(f)
T = 3.9
Q
h_b

Figures

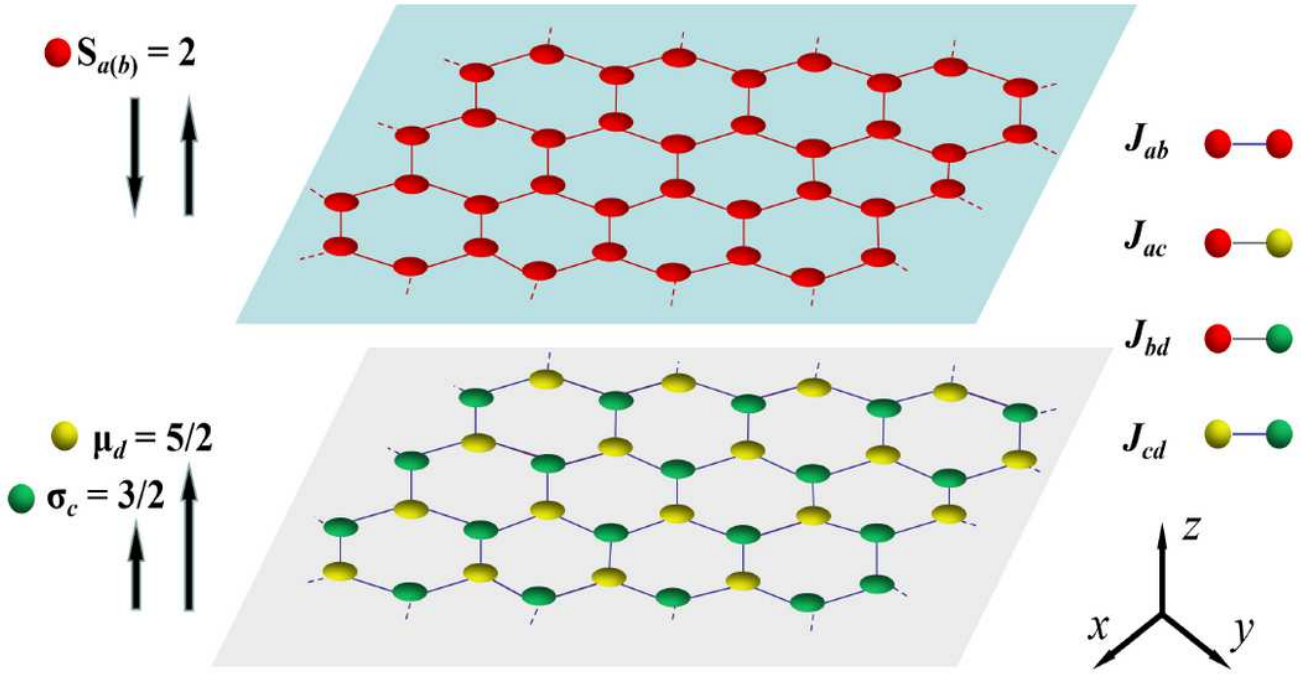

Figure 1

Schematic of an antiferromagnetic/ferromagnetic mixed-spin(5/2, 2, 3/2) Ising model with the YMnO3/FM bilayer structure. Four exchange interactions are considered in the structure. Jab and Jcd denote the intralayer antiferromagnetic and ferromagnetic exchange interactions of different spins in the top layer between sublattices a and b, and in the bottom layer between sublattices c and d, respectively. Jac and Jbd represent the interlayer exchange interactions between sublattices a and c, b and d, namely.

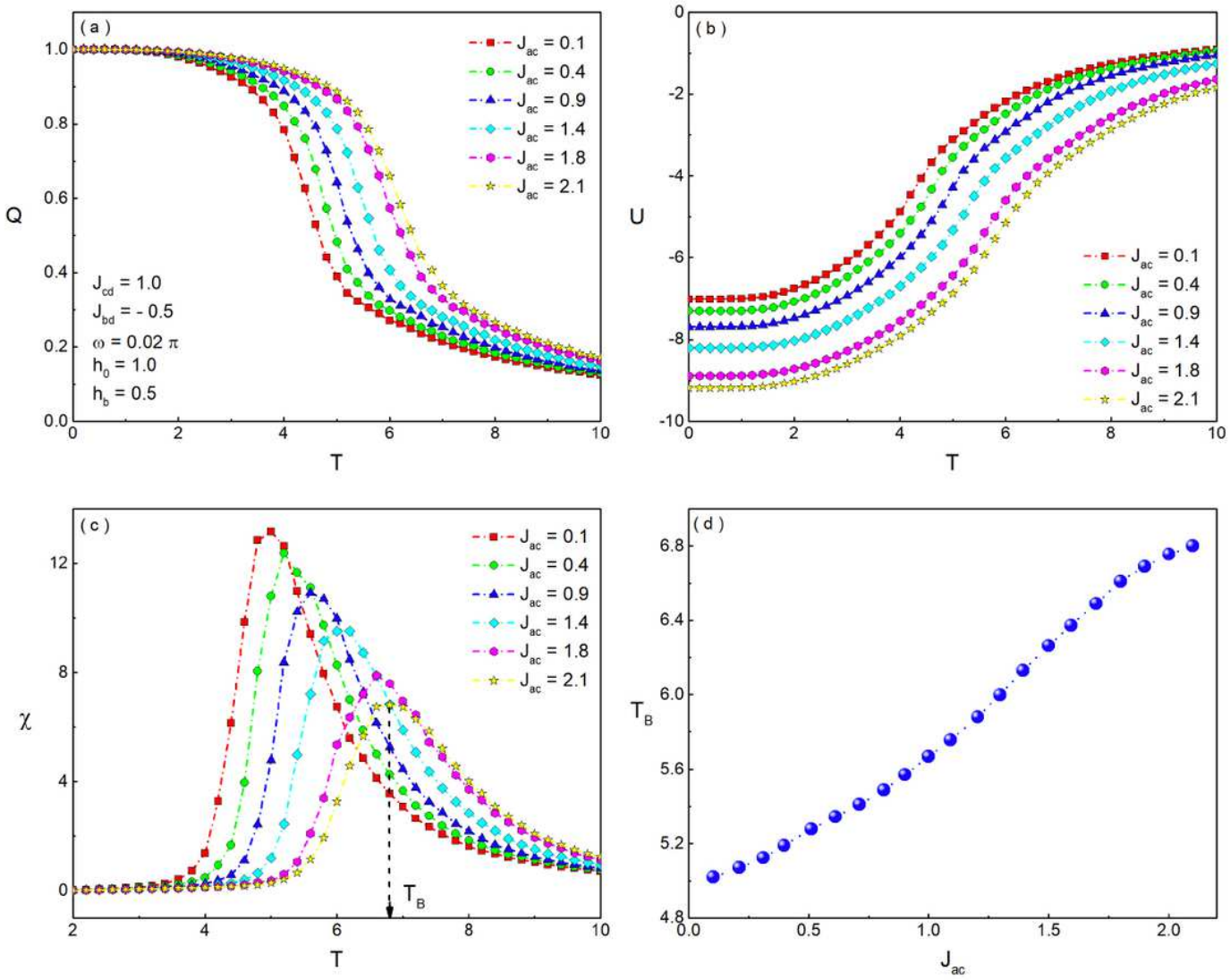

Figure 2

The temperature dependences of Q, U, χ, and the diagram of TB for different Jac with Jcd = 1.0, Jbd = -0.5, ω = 0.02π, h0 = 1.0, and hb = 0.5.

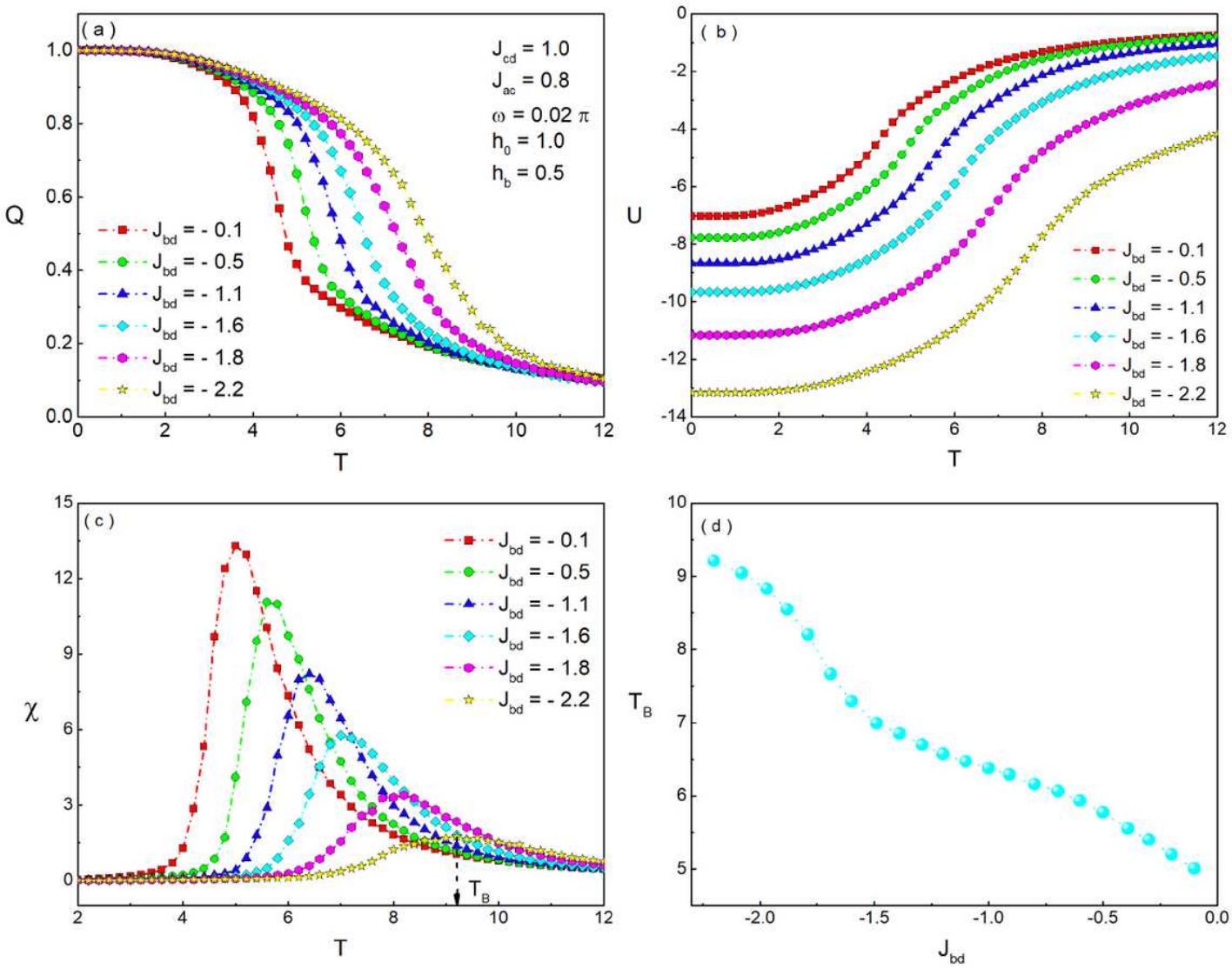

Figure 3

The temperature dependences of Q, U, χ and the diagram of TB for different Jbd on the condition of Jcd = 1.0, Jac = 0.8, ω = 0.02π, h0 = 1.0, and hb = 0.5.

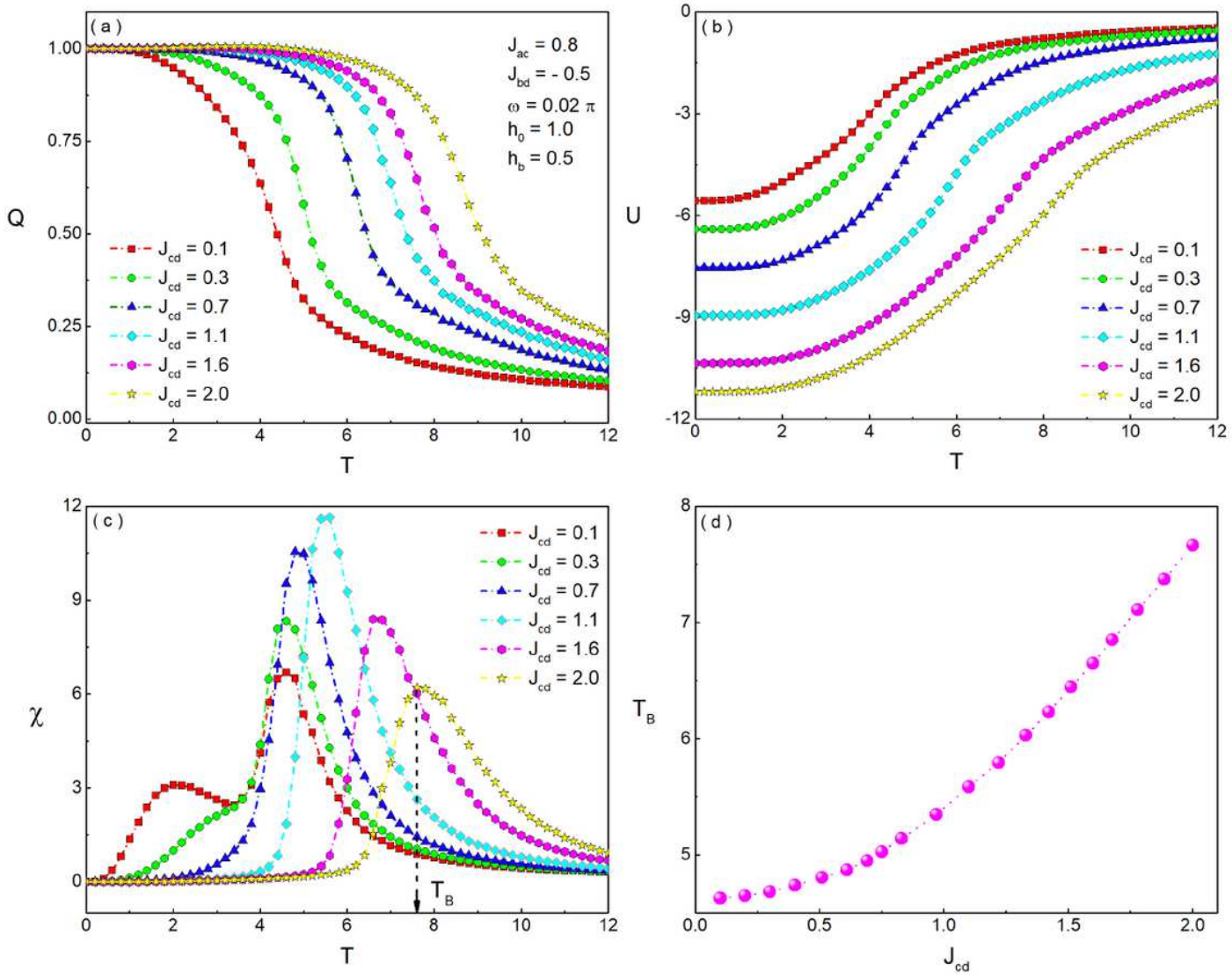

Figure 4

The temperature dependences of Q, U, χ and the diagram of TB for different Jcd with Jac = 0.8, Jbd = -0.5, ω = 0.02π, h0 = 1.0, and hb = 0.5.

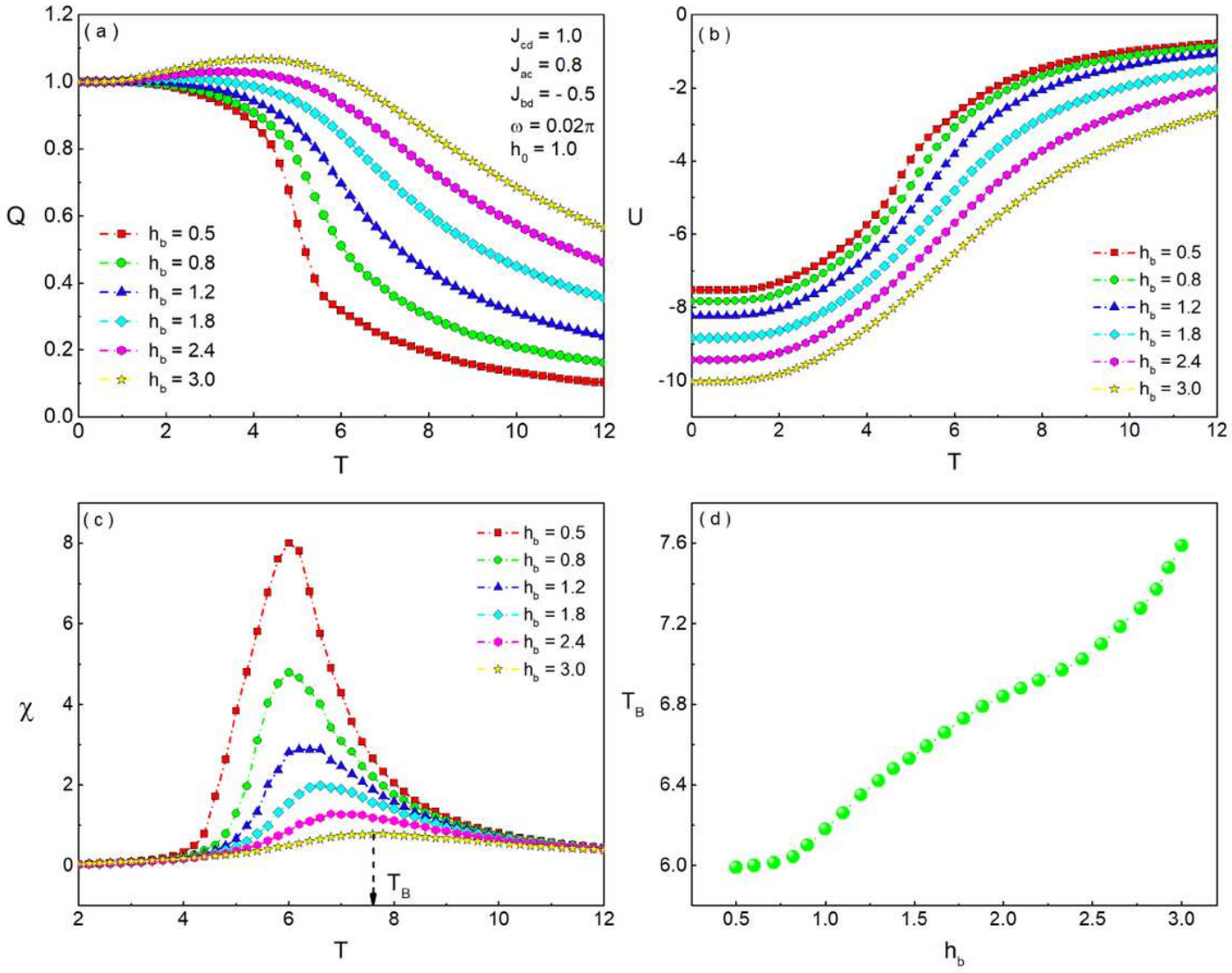

Figure 5

The temperature dependences of Q, U, χ and the diagram of TB for different hb with Jcd = 1.0, Jac = 0.8, Jbd = -0.5, ω = 0.02π, and h0 = 1.0.

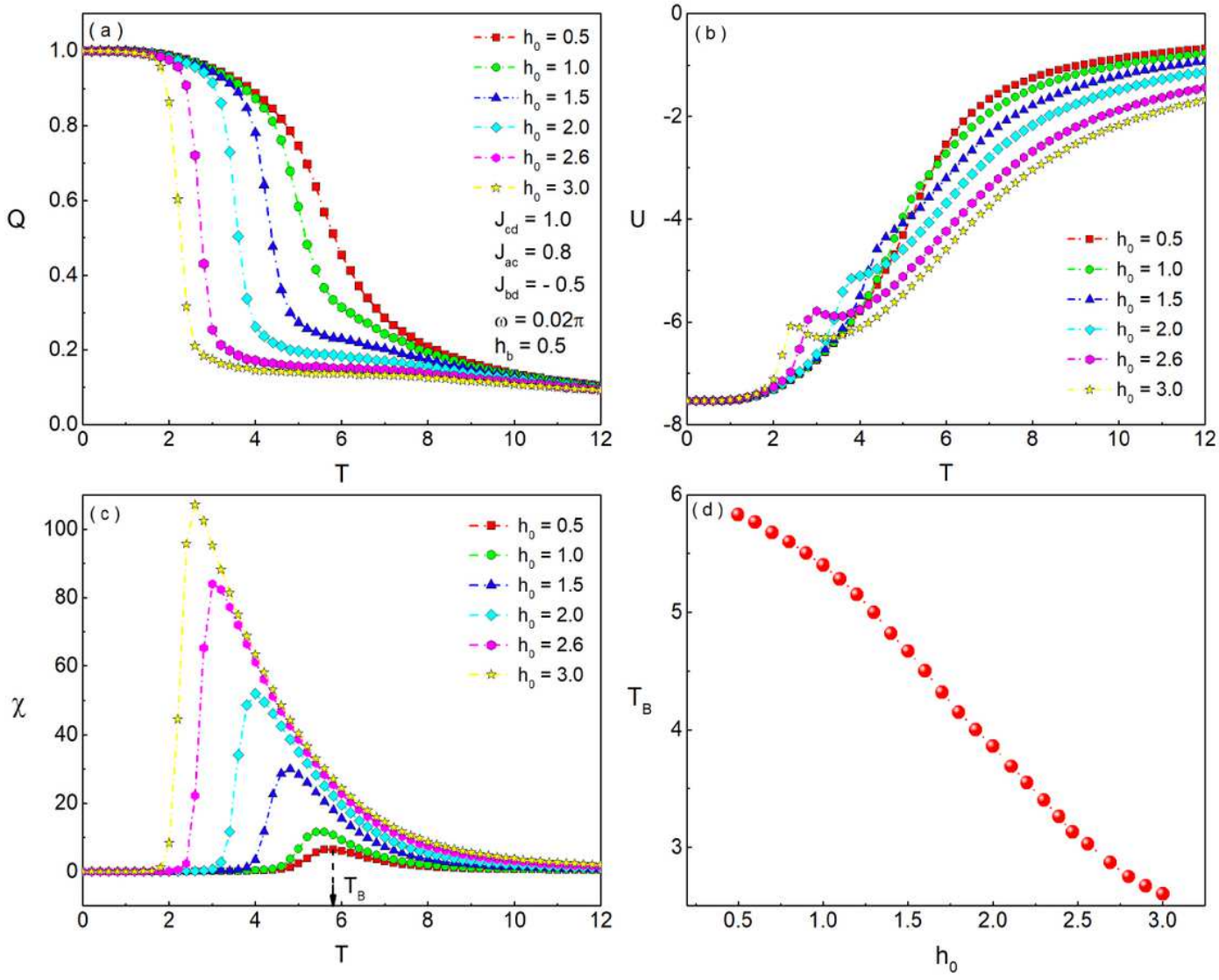

Figure 6

The temperature dependences of Q, U, χ and the diagram of TB for different h0 with Jcd = 1.0, Jac = 0.8, Jbd = -0.5, ω = 0.02π and hb = 0.5.

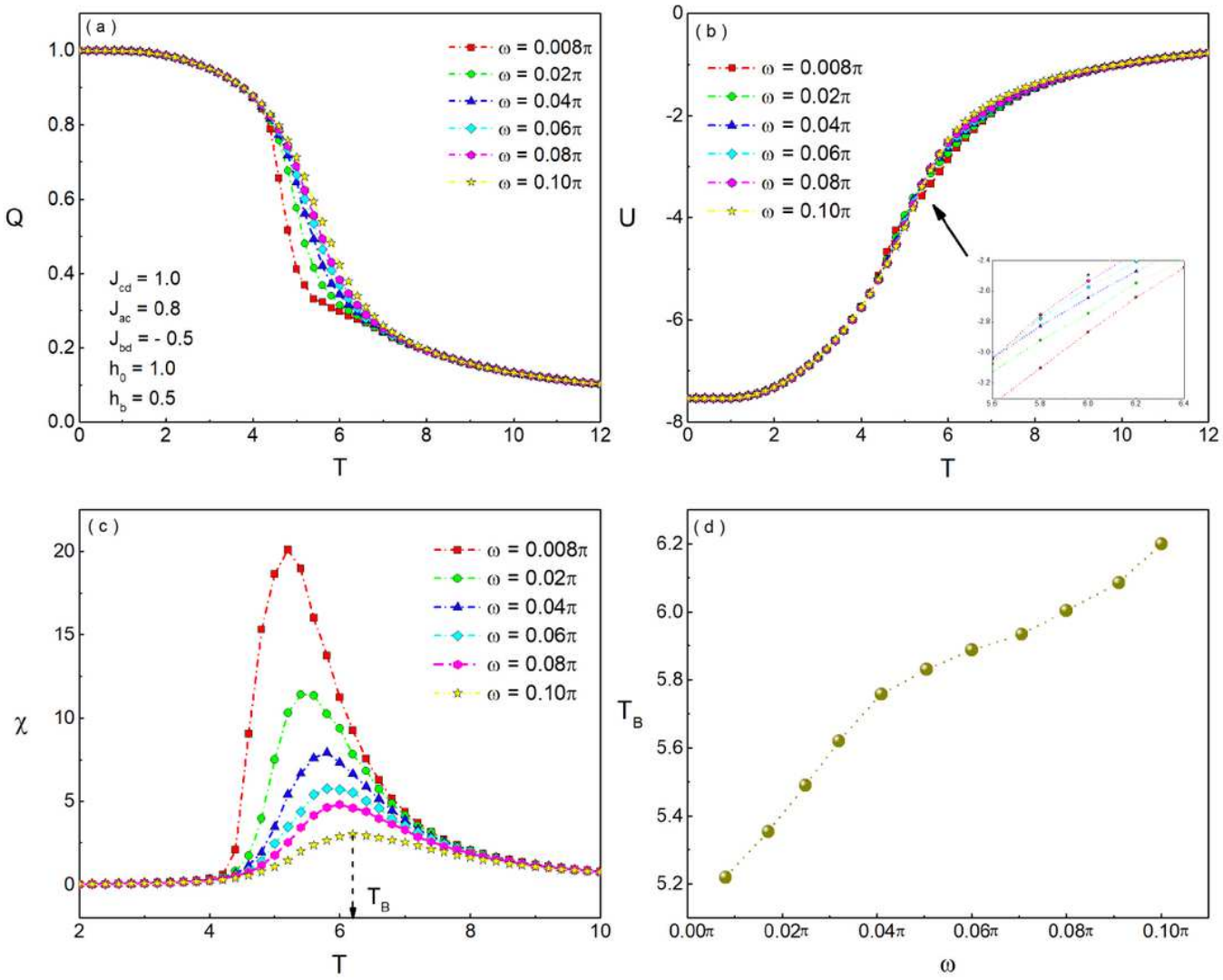

Figure 7

The temperature dependences of Q, U, χ and the diagram of TB for different ω with Jcd = 1.0, Jac = 0.8, Jbd = -0.5, h0 = 1.0 and hb = 0.5.

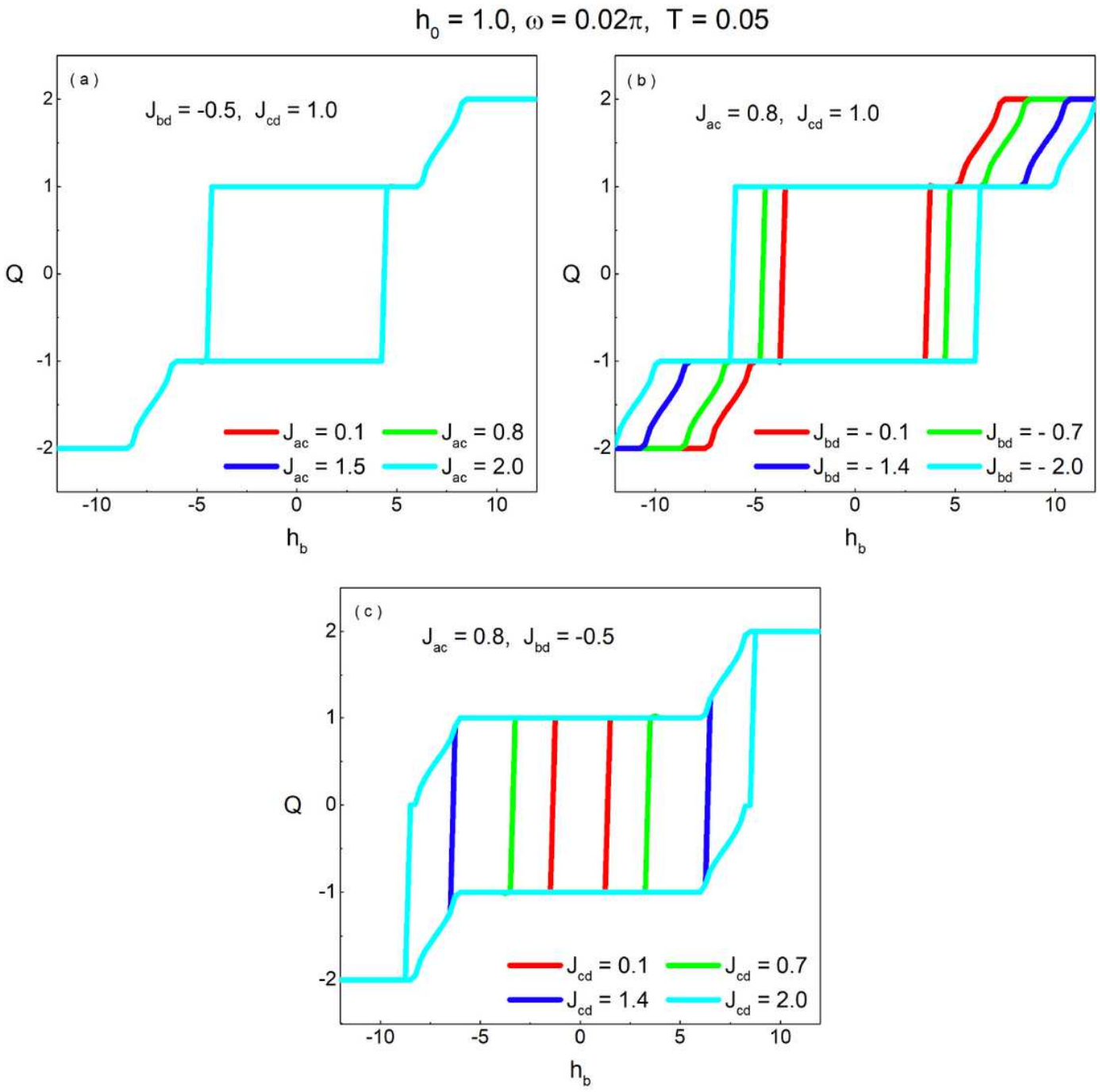

Figure 8

The hysteresis loops of the anferromagnetic/ferromagnetic bilayer for different values of (a) Jac with Jbd = -0.5, Jcd = 1.0, h0 = 1.0, ω = 0.02π, T = 0.05, (b) Jbd with Jac = 0.8, Jcd = 1.0, h0 = 1.0, ω = 0.02π, and T = 0.05, (c) Jcd with Jac = 0.8, Jbd = -0.5, h0 = 1.0, ω = 0.02π, and T = 0.05.

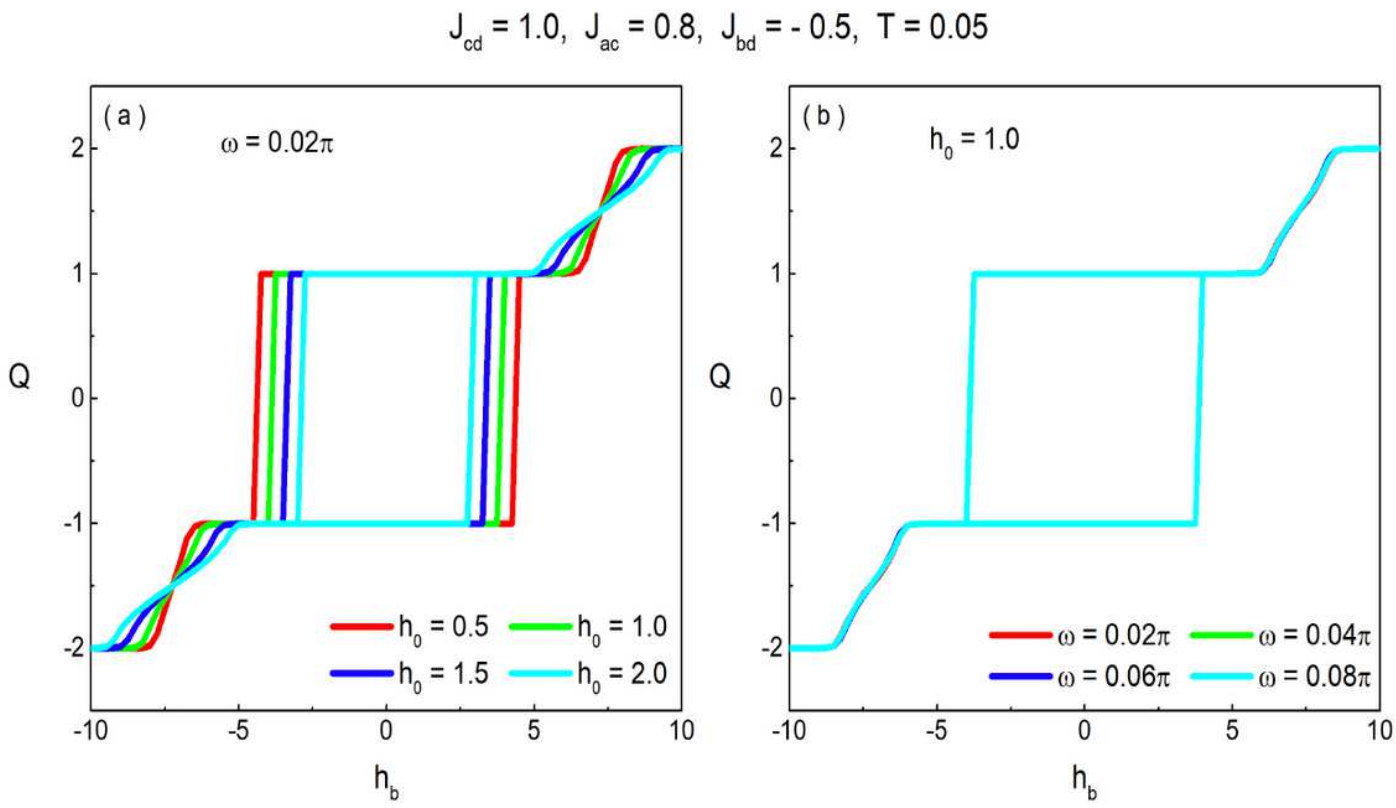

Figure 9

The hysteresis loops of the anferromagnetic/ferromagnetic bilayer for different values of (a) h0 with ω = 0.02π, Jcd = 1.0, Jac = 0.8, Jbd = -0.5, and T = 0.05, (b) ω with h0 = 1.0, Jcd = 1.0, Jac = 0.8, Jbd = -0.5, and T = 0.05.

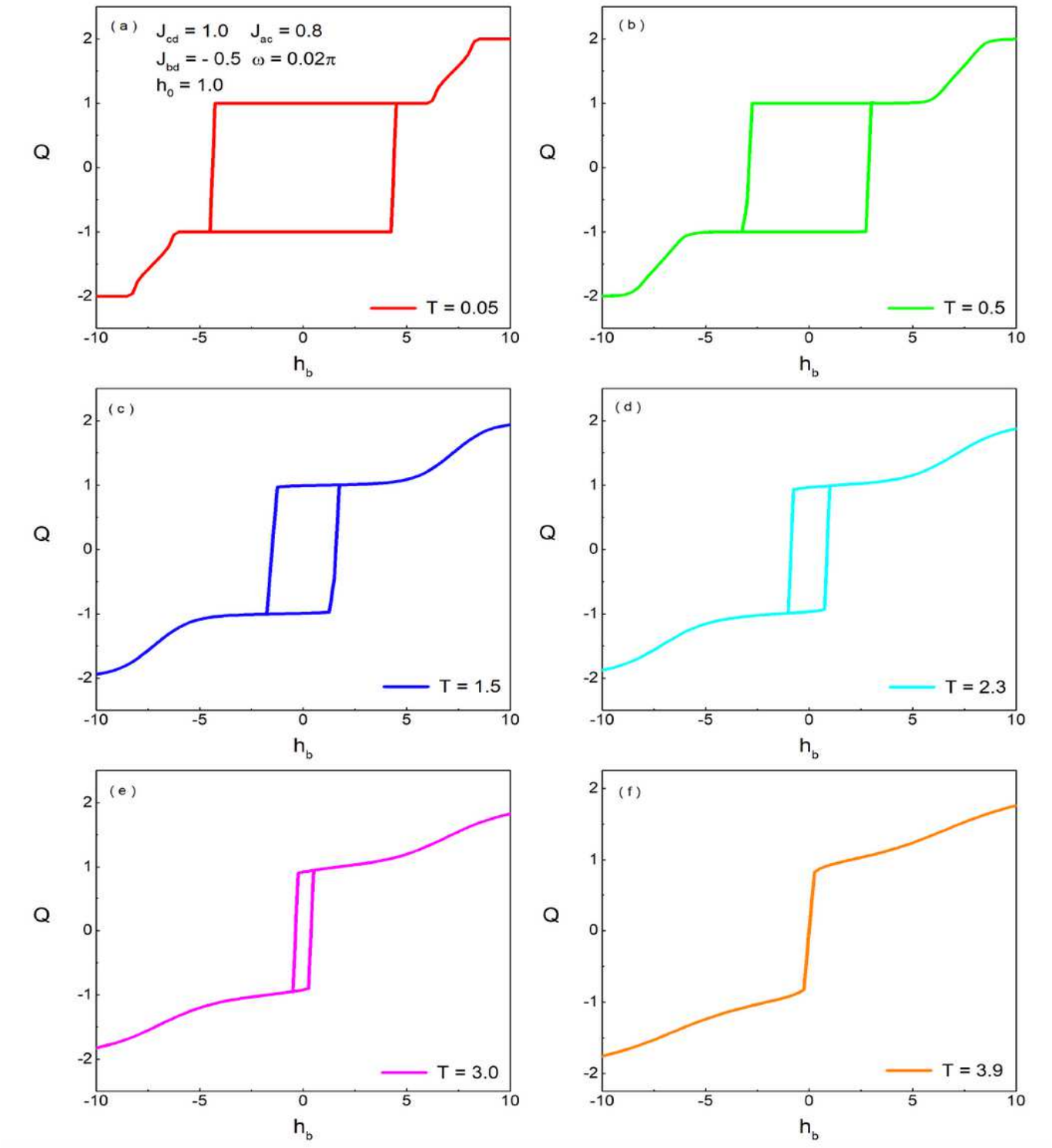

Figure 10

The hysteresis loops of the anferromagnetic/ferromagnetic bilayer for different values of T with Jcd = 1.0, Jac = 08, Jbd = -0.5, ω = 0.02π, and h0 = 1.0.